Tracking POPs in Global Air from the first 10 years of the GAPS Network (2005 to 2014)

Supplementary Information

Jasmin K Schuster[1*], Tom Harner[1], Anita Eng[1], Cassandra Rauert[1,2], Ky Su[1], Keri C. Hornbuckle[3], Connor W. Johnson[3]

[1] Air Quality Processes Research Section, Environment and Climate Change Canada, Toronto, Ontario, M3H 5T4. Canada
[2] Queensland Alliance for Environmental Health Sciences (QAEHS), The University of Queensland, Woolloongabba, Queensland, 4102, Australia
[3] Department of Civil and Environmental Engineering and IIHR-Hydroscience and Engineering, The University of Iowa, Iowa City, Iowa 52242, United States of America
*jasmin.schuster@canada.ca

Contents

Figure S1. Timeline for compounds listed under the Stockholm Convention on POPs

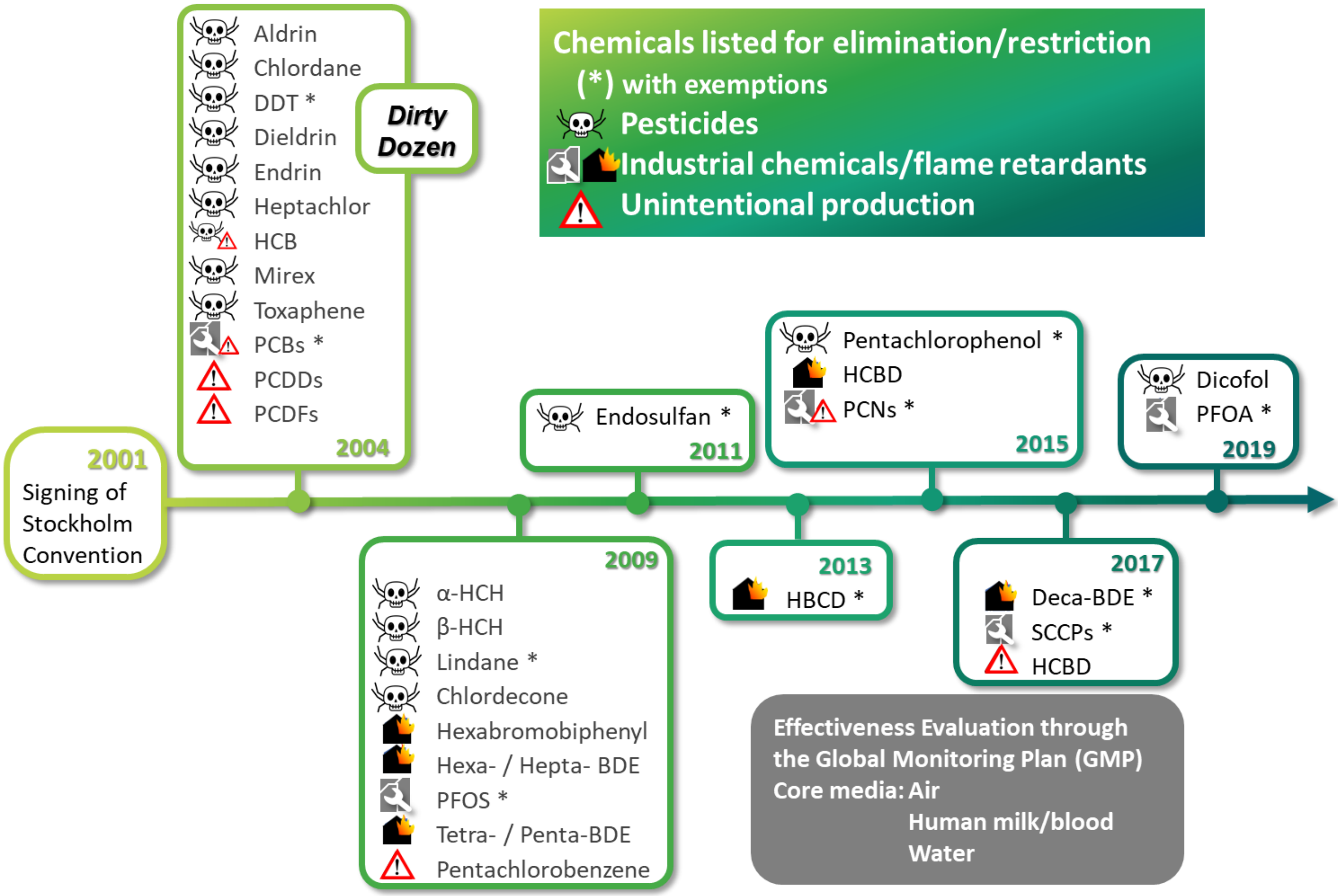

Figure S2. Map of all GAPS sites

Map of all GAPS sites 2005-2014 with Site ID and site names (below). Additional site details are available in an Excel file included in the SI. GAPS sites with long-term POP data for temporal trend analysis are marked yellow. GAPS sites that are in operation as of summer 2021 are marked with a star in the list (★).

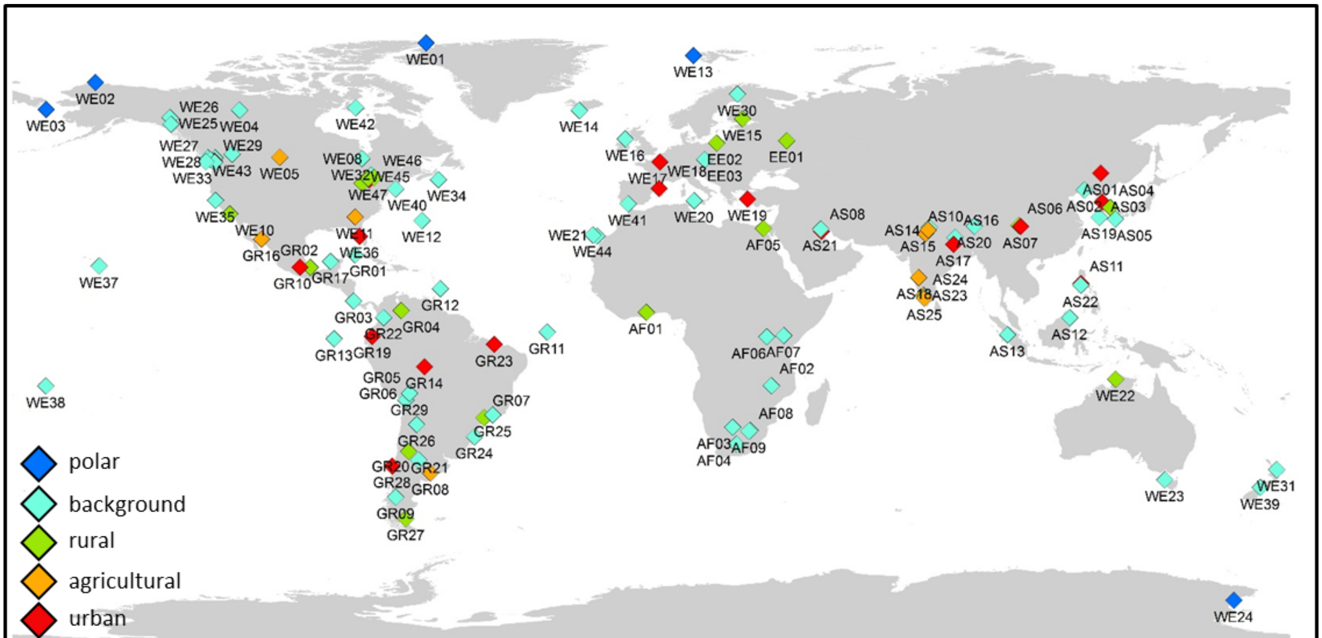

AF01	Accra	AS20	Nam Co, Tibet	★GR22	Manizales	WE21	Telde, Las Palmas
AF02	Lilongwe	★AS21	Abdaly	★GR23	São Luis do Maranha	★WE22	Darwin
AF03	Kalahari	AS22	Tagaytay City	★GR24	São Jose dos Ausentes	★WE23	Cape Grim
★AF04	De Aar	AS23	Ooty	★GR25	Itatiaia	WE24	Mario Zucchelli Station, Antarctica
AF05	Cairo	AS24	Coimbatore, Tamil Nadu	★GR26	Salta	★WE25	Little Fox Lake, Yukon
★AF06	Bukasa Island	AS25	Aliyar Nagar	★GR27	Rio Gallegos	★WE26	Dyea, Alaska
★AF07	Mt. Kenya	EE01	Danki	★GR28	Concepción	WE27	Cortes Island, British Columbia
AF08	Vanderbijlpark	EE02	Pomlewo (near Gdańsk)	★GR29	Chacaltaya	WE28	Lasqueti Island, BC
AF09	Vredefort Dome	★EE03	Košetice	★WE01	Alert, Nunavut	WE29	Saturna Island, British Columbia
AS01	Harbin, Heilong Jiang	GR01	La Palma	★WE02	Barrow, Alaska	★WE30	Pallas
AS02	Dalian, Liaoning	GR02	Veracruz	WE03	St. Lawrence Island, Alaska	WE31	North Island
AS03	Seoul	★GR03	Tapanti National Park	WE04	Snare Rapids, Northwest Territories	★WE32	Fraserdale, ON
AS04	Pohang	★GR04	Arauca	★WE05	Bratt's Lake, Saskatchewan	★WE33	Ucluelet, BC
AS05	Kumamoto	GR05	Huayna Potosí 5200 m a.s.l., La Paz	★WE06	Whistler, British Columbia	★WE34	Sable Island, NS
AS06	Mt. Qingcheng, Sichuan	GR06	Chungara Lake	WE07	Vancouver, British Columbia	★WE35	Point Reyes, CA
AS07	Chengdu, Sichuan	GR07	Indaiatuba, São Paulo	WE08	Dorset, Ontario	★WE36	Sydney, Florida
AS08	Kuwait City	GR08	Bahia Blanca	★WE09	Downsview, Ontario	★WE37	Mauna Loa Obs, Hilo, Hawaii
AS09	East Arjun Nagar	GR09	Coyhaique	WE10	Simi Valley, California	★WE38	Tula, American Samoa
AS10	Bawana	GR10	Tlahuac, Mexico City	WE11	Athens, Georgia	★WE39	Temple Basin, Arthur's Pass
★AS11	Manila	GR11	St. Peter and St. Paul Rocks	★WE12	Tudor Hill	★WE40	Groton, CT
★AS12	Danum Valley	★GR12	Ragged Point, St. Philip	★WE13	Ny-Ålesund	★WE41	Doñana National Park
★AS13	Bukit Kototabang	★GR13	Santa Cruz Island (Galapagos Islands)	★WE14	Stórhöfði	WE42	Coral Harbour, NU
AS14	Kaddu Khal	GR14	Porto Velho	WE15	Hollola	★WE43	Mount Revelstoke, BC
AS15	Laksar	★GR16	Valley of the Yaqui in Sonora	★WE16	Malin Head	★WE44	Izana
AS16	Dhulikhel	GR17	Celestún in Yucatan	★WE17	Paris	★WE45	Longwoods
AS17	Patna	★GR19	Quito	WE18	Barcelona	★WE46	Warsaw Caves
AS18	Mudhol	★GR20	Pierre Auger Observatory (Patagonia Flats)	WE19	Izmir	★WE47	Egbert / CARE Station
★AS19	Gosan, Jeju Island	★GR21	Mendoza Province	WE20	Isola Marettimo		

Text S1. Effective air volume calculation

With its start in 2005, the GAPS network aimed to deliver global information on POP concentrations in air. PUF-PAS were selected as a cost-effective method with low logistical requirements. Site- and sample-specific sampling rate (R) values were derived from depuration compounds (DCs), that were spiked on the PUF disk prior to deployment. R values were estimated from the loss of DCs during deployment [2]. While DC derived R values reflect the diverse meteorological conditions at the different sampling sites, this method introduces additional uncertainty. It was found that the loss of depuration compounds should be in a window of 20-60% to minimize the influence of the analytical uncertainty [2, 6]. Some sites show meteorological conditions (i.e. extreme temperatures and wind speeds) that make it difficult to attain accurate R values based on these requirements.

Herkert et al. developed a model and online tool based on DC-derived sampling rates from the GAPS network and meteorological data. Site and compound specific sampling rates are estimated from sampling dates and location coordinates [3-5]. The resulting model R values are not considerably different between the majority of sites, with 90% of values in the range 4 ± 2 m3/day, consistent with previous reporting under the GAPS program (Figure S3). For this paper and going forward all GAPS legacy POP concentrations in air are estimated using these model R values. This reduces the analytical costs associated with DCs and their additional analysis time. It also reduces uncertainty in derived R-values between sampling and processing years and allows the analysis of temporal trends within the GAPS data for the sampling periods 2005-2014. Another environmental benefit to moving away from DCs, is that it eliminates the emission of POPs spiked into the PUF disks to ambient air.

When using the model, some sites showed unexpectedly low sampling rates due to low model wind speeds. It was determined that this is due to the model assuming forest cover, whereas in reality the sites were located in areas cleared of trees, and therefore experience usual wind speeds. Further inspection indicated that this was mainly a problem with coastal and mountain sites that were adjacent to forests. Low model grid resolution had assigned dampened wind speeds more typical for forest-covered areas to these sites.

Sampling rates for these few sites with extremely low modelled wind speed were adjusted based on local wind speed data (NOAA data files [7]) and the wind speed [WS] ~ sampling rate [R] relationship from the modelled data:

Equation 1. **R (m3/day) = 1.6087 * [WS (m/s)]$^{0.6265}$**

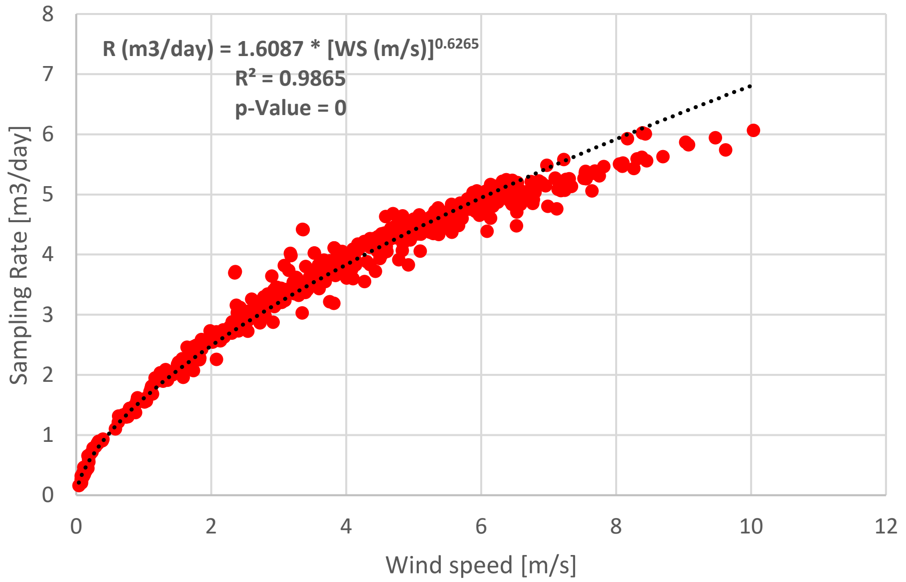

The template based on Shoeib and Harner was used to estimate effective air volumes from the modelled sampling rates [8, 9].

Figure S3. Comparison between R_{DC} and R_{model}

The average sampling rates for 2011 derived from depuration compounds (R_{DC}) [2] and from the Herkert et al. online model (R_{model}) [3-5] are presented at the individual GAPS sites. Details are in Text S1.

Greater discrepancies observed at a few of the polar sites is likely attributed to challenges (e.g. slow off-gassing) with using DCs at colder temperatures.

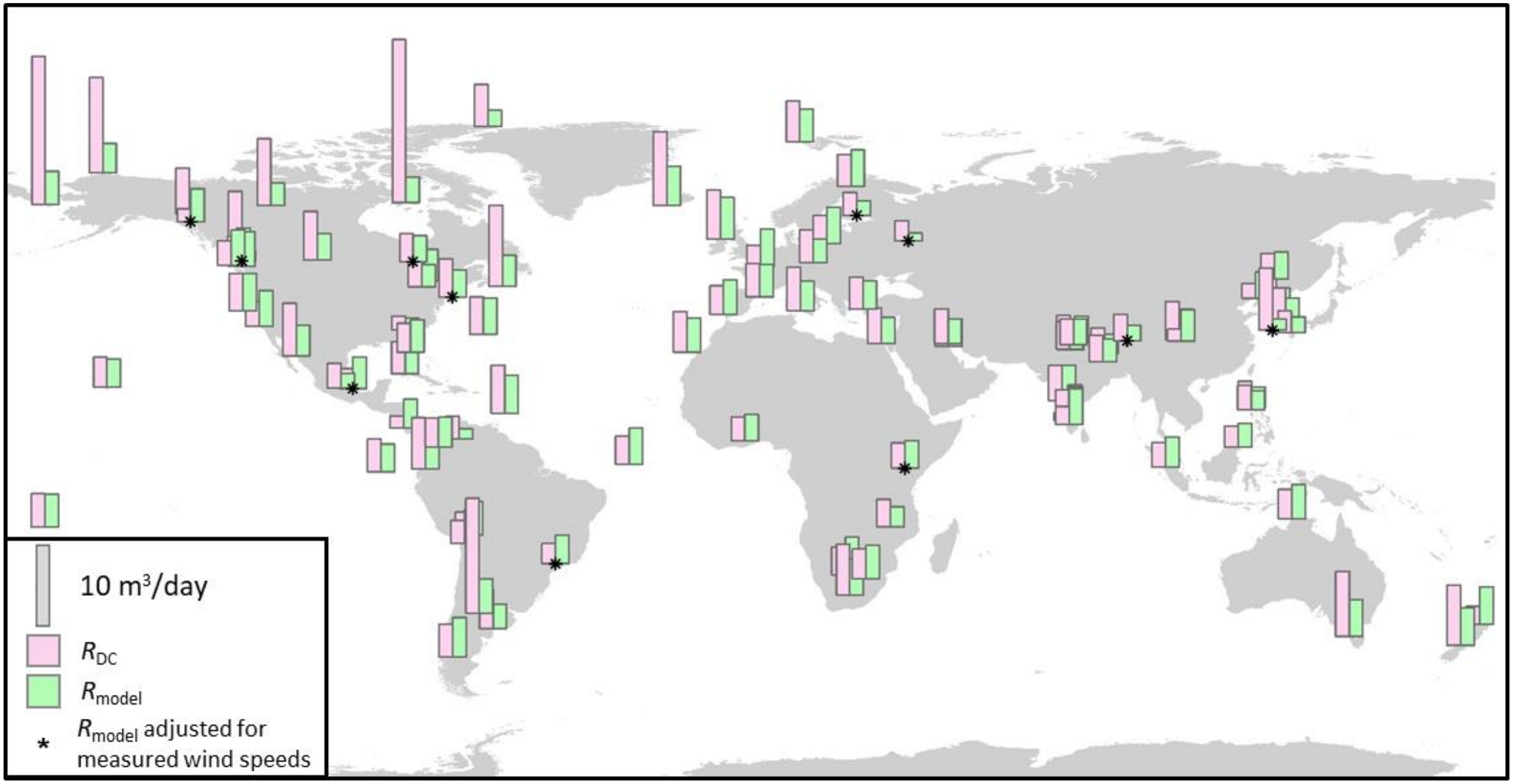

Figure S4. Bee swarm-boxplot-summary of the range of global concentrations of $\sum_7$PCB, α-HCH, γ-HCH, Endosulfan I, Endosulfan II and Endosulfan SO_4 for GAPS 2005-2006

The plot depicts the single data points and the boxplots marking the median, 25th and 75th percentile (whiskers marking the 10th and 90th percentile).

Site types: PO= polar, BA = background, RU = rural, AG = agricultural, UR = urban

UNEP regional groups: Africa = African Group, Asia = Asia and Pacific Group, CEE = Central and Eastern European Group, GRULAC = Group of Latin America and Caribbean countries, WEOG = Western European and Others Group

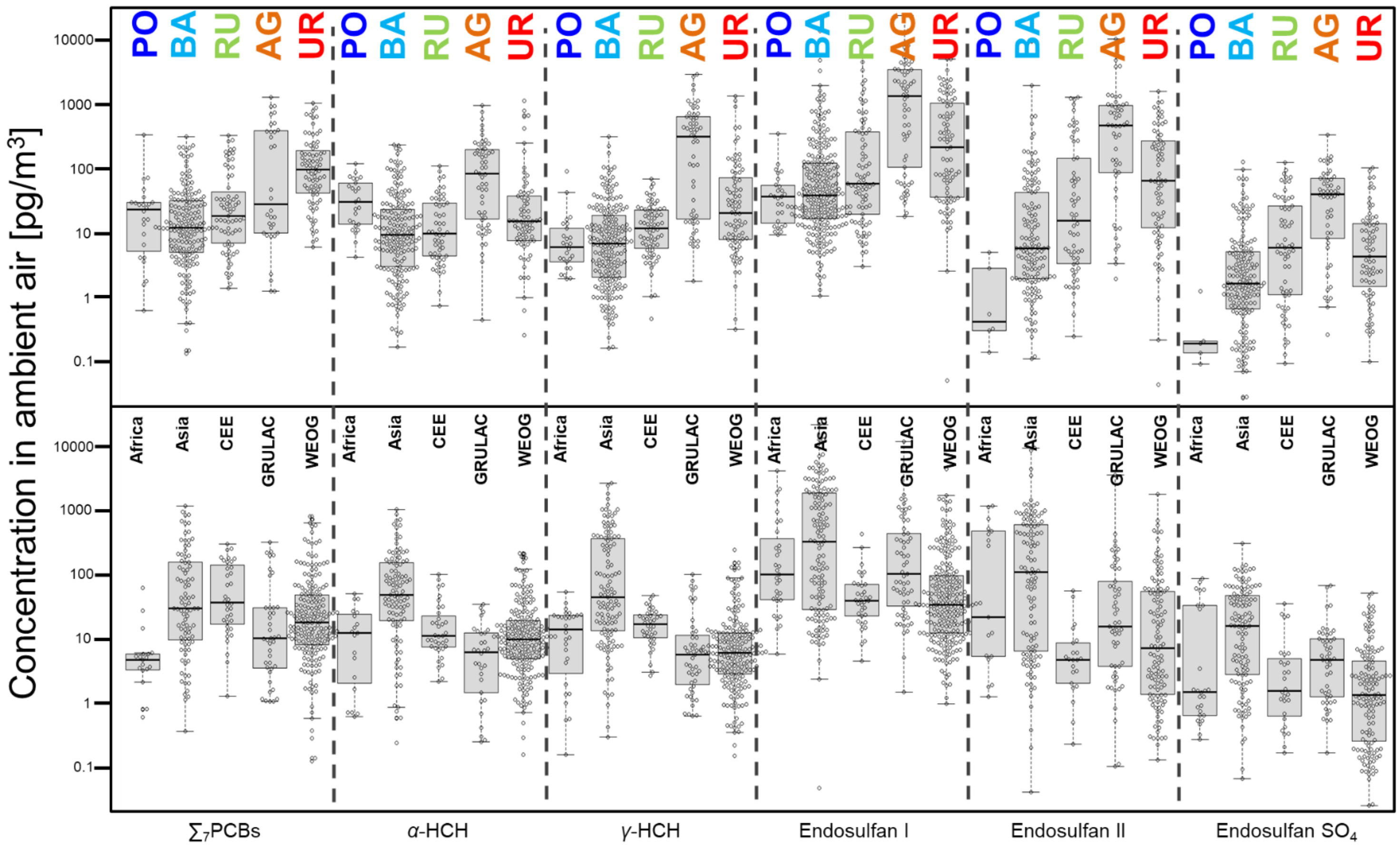

Figure S5. Bee swarm-boxplot-summary of the range of global concentrations of the individual PCB congener PCB 28/52/101/118/138/153/180

Figure S5a. Global concentrations resolved by site type for GAPS 2005-2007 and GAPS 2011/2014

The plot depicts the single data points and the boxplots marking the median, 25th and 75th percentile (whiskers marking the 10th and 90th percentile).

Site types: PO= polar, BA = background, RU = rural, AG = agricultural, UR = urban

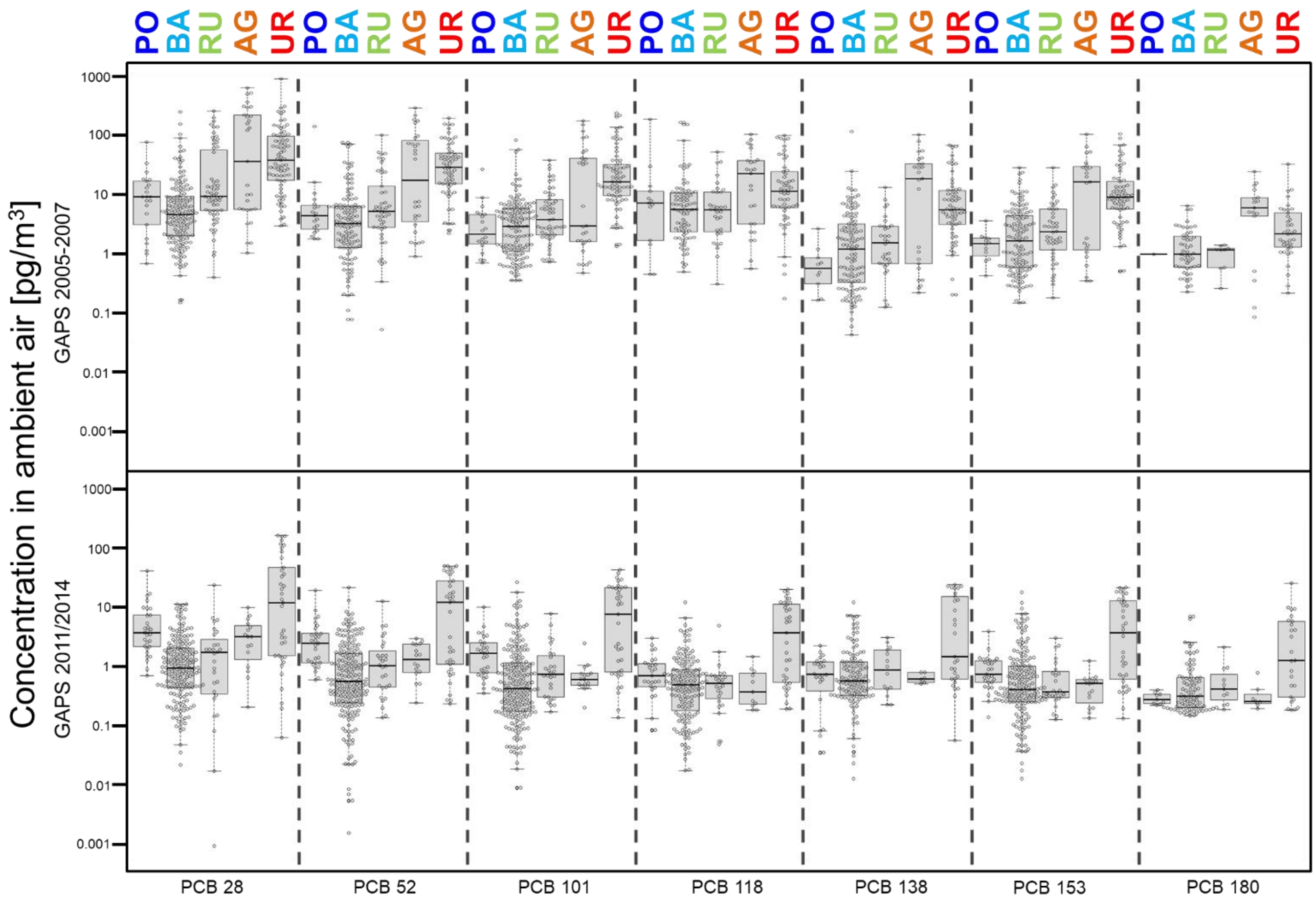

Figure S5b. Global concentrations resolved by UNEP regional group for GAPS 2005-2007 and GAPS 2011/2014

The plot depicts the single data points and the boxplots marking the median, 25th and 75th percentile (whiskers marking the 10th and 90th percentile).

UNEP regional groups: Africa = African Group, Asia = Asia and Pacific Group, CEE = Central and Eastern European Group, GRULAC = Group of Latin America and Caribbean countries, WEOG = Western European and Others Group

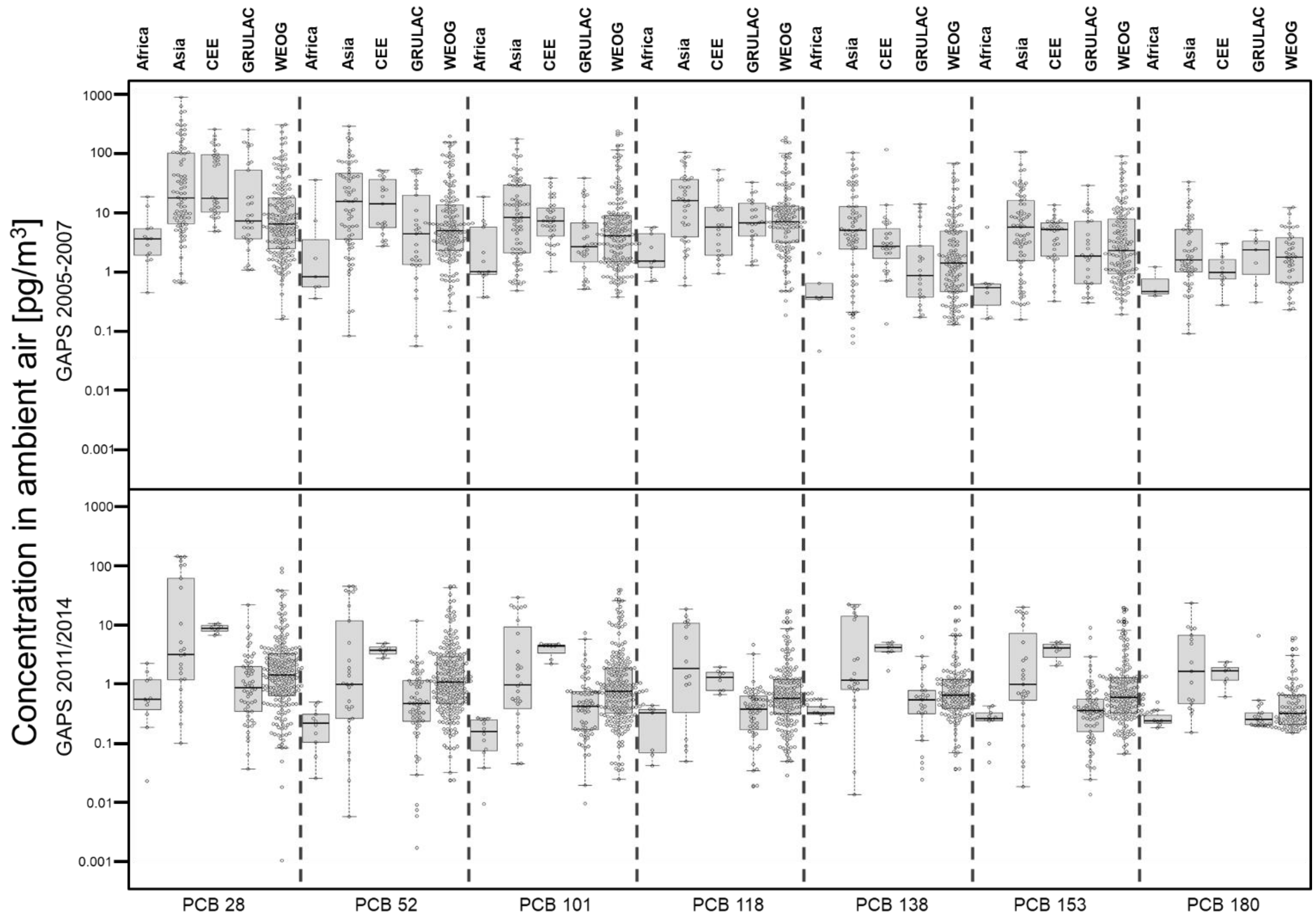

Figure S6. Bee swarm-boxplot-summary of the range of global concentrations of Dieldrin

Figure S6a. Global concentrations resolved by site type for GAPS 2005-2007 and GAPS 2011/2014

The plot depicts the single data points and the boxplots marking the median, 25th and 75th percentile (whiskers marking the 10th and 90th percentile).

Site types: PO= polar, BA = background, RU = rural, AG = agricultural, UR = urban

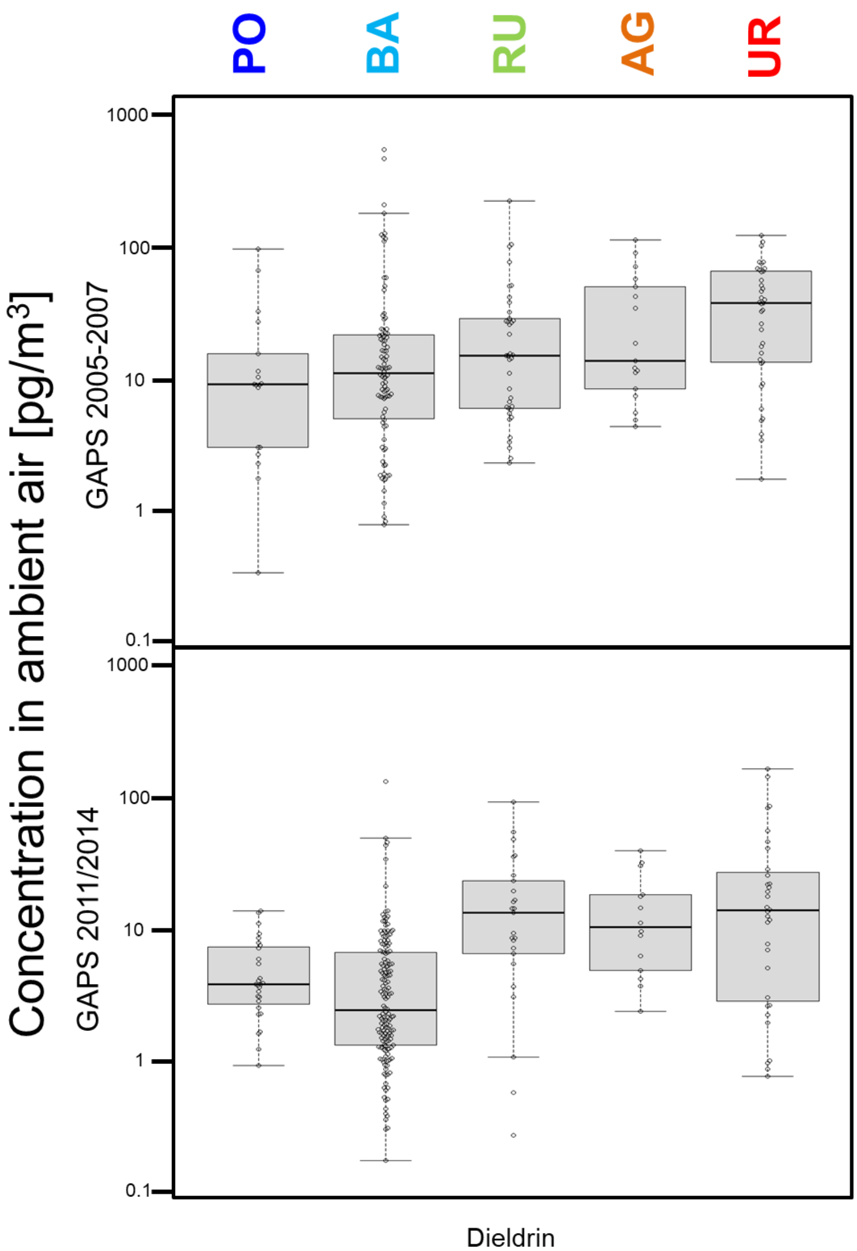

Figure S6b. Global concentrations resolved by UNEP regional group for GAPS 2005-2007 and GAPS 2011/2014

The plot depicts the single data points and the boxplots marking the median, 25th and 75th percentile (whiskers marking the 10th and 90th percentile).

UNEP regional groups: Africa = African Group, Asia = Asia and Pacific Group, CEE = Central and Eastern European Group, GRULAC = Group of Latin America and Caribbean countries, WEOG = Western European and Others Group

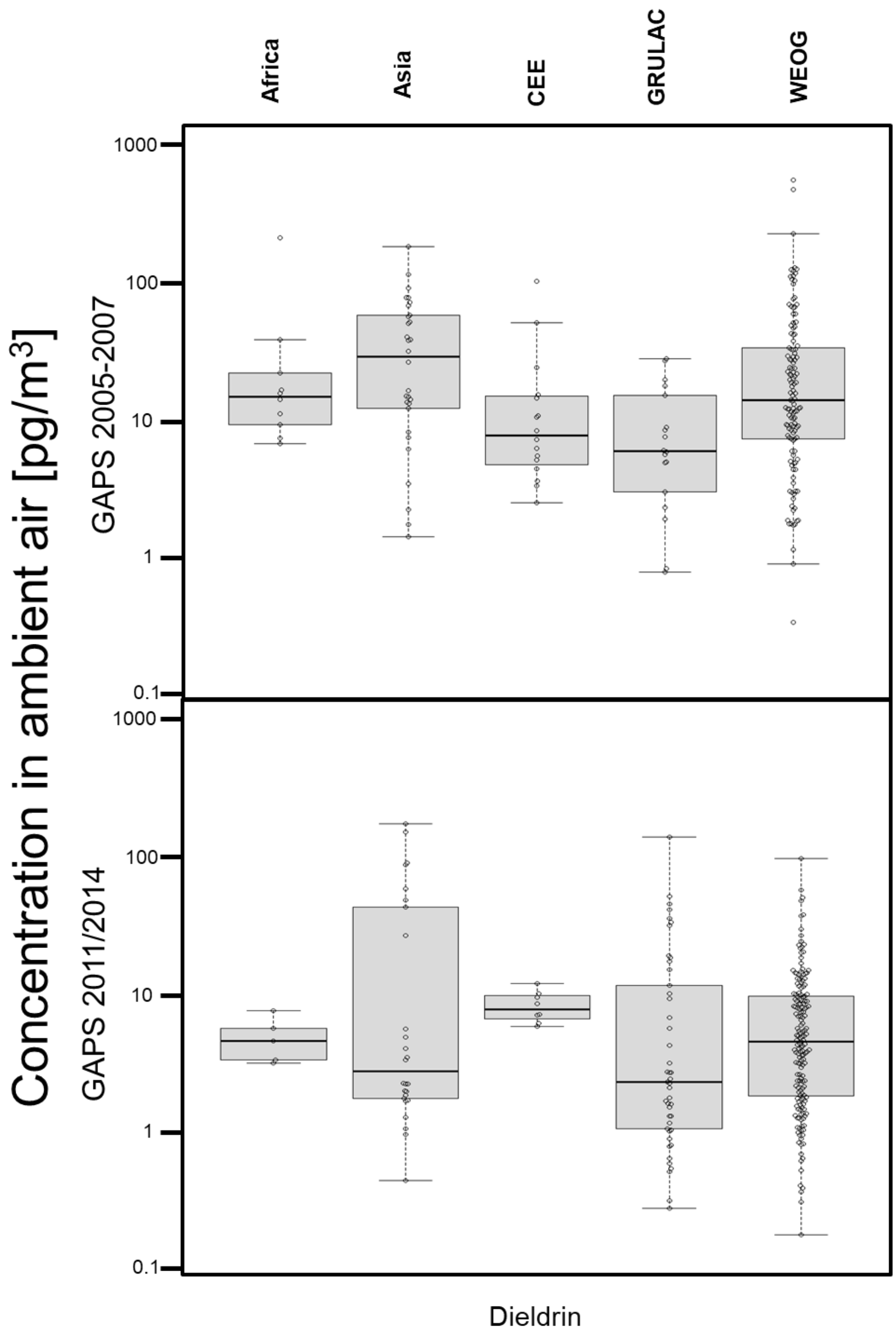

Figure S7. Bee swarm-boxplot-summary of the range of global concentrations of *cis*-Chlordane, *trans*-Chlordane, *trans*-Nonachlor, Heptachlor and Heptachlor epoxide

Figure S7a. Global concentrations resolved by site type for GAPS 2005-2007 and GAPS 2011/2014

The plot depicts the single data points and the boxplots marking the median, 25th and 75th percentile (whiskers marking the 10th and 90th percentile).

Site types: PO= polar, BA = background, RU = rural, AG = agricultural, UR = urban

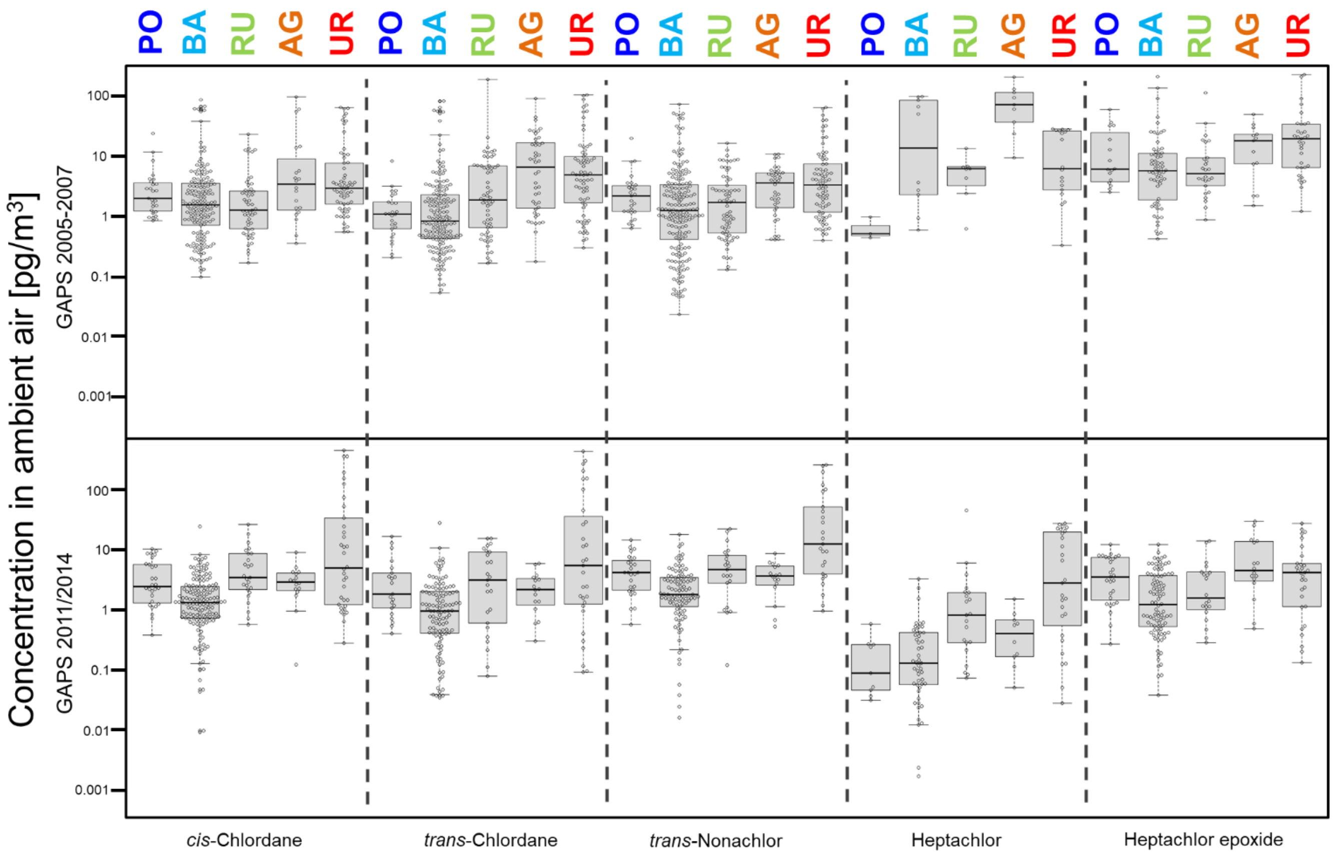

Figure S7b. Global concentrations resolved by UNEP regional group for GAPS 2005-2007 and GAPS 2011/2014

The plot depicts the single data points and the boxplots marking the median, 25th and 75th percentile (whiskers marking the 10th and 90th percentile).

UNEP regional groups: Africa = African Group, Asia = Asia and Pacific Group, CEE = Central and Eastern European Group, GRULAC = Group of Latin America and Caribbean countries, WEOG = Western European and Others Group

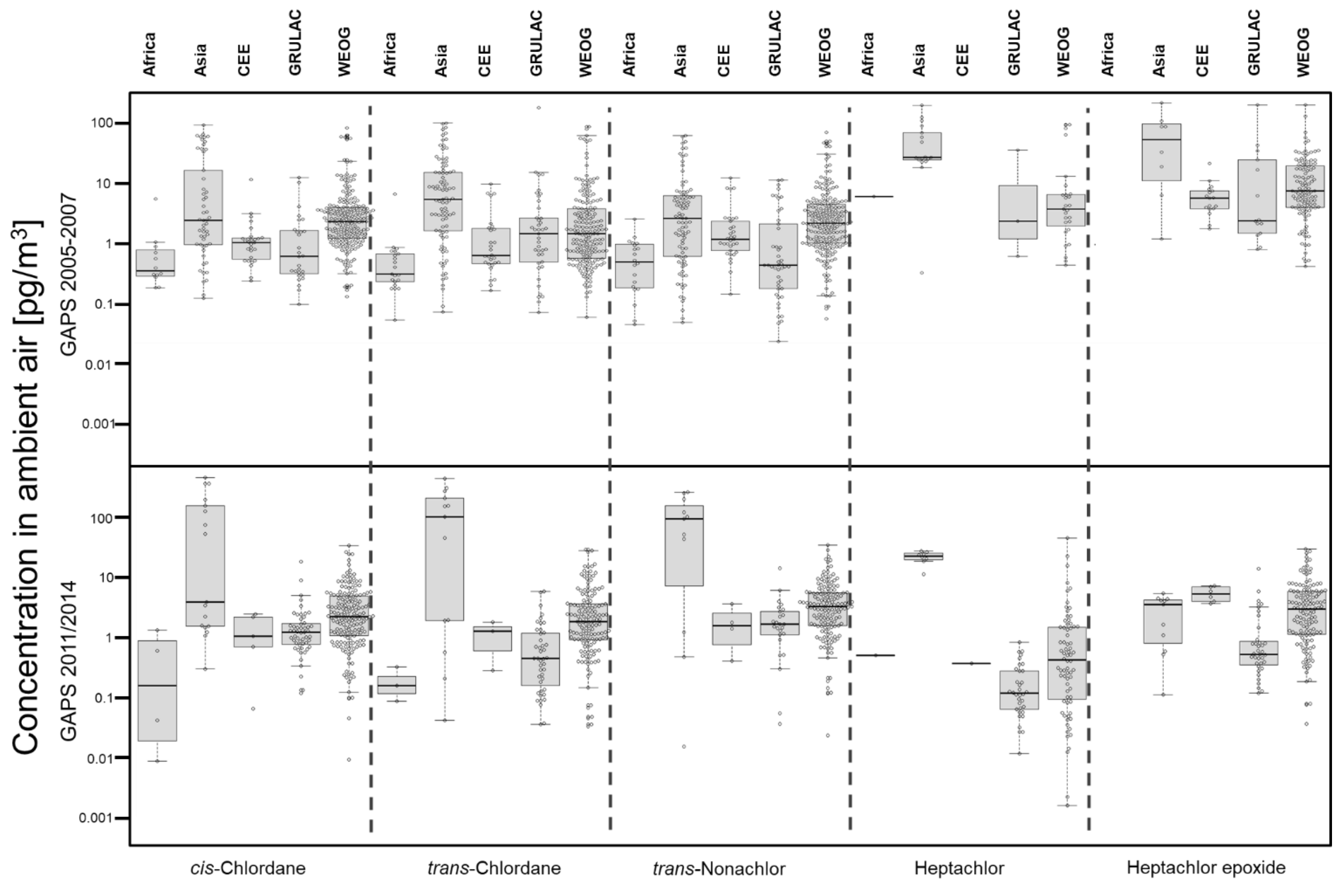

Figure S8. Bee swarm-boxplot-summary of the α-HCH fractions

The fraction of α-HCH was estimated for GAPS 2005-2007 and GAPS 2011/2014 for all samples with both α-HCH and γ-HCH above MDL. The plot depicts the single data points and the boxplots marking the median, 25th and 75th percentile (whiskers marking the 10th and 90th percentile).

Site types: PO= polar, BA = background, RU = rural, AG = agricultural, UR = urban

UNEP regional groups: Africa = African Group, Asia = Asia and Pacific Group, CEE = Central and Eastern European Group, GRULAC = Group of Latin America and Caribbean countries, WEOG = Western European and Others Group

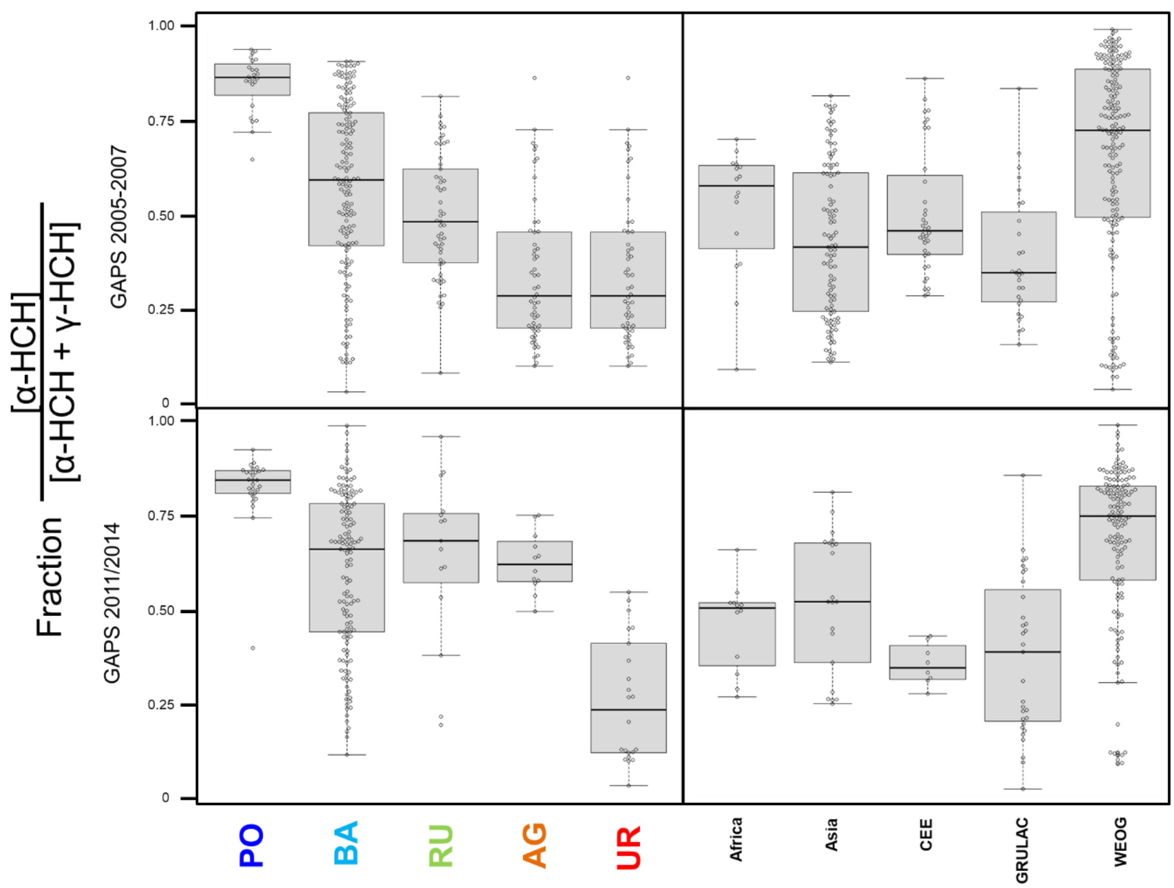

Figure S9. Bee swarm-boxplot-summary of the Endosulfan I fractions

The fraction of Endosulfan I was estimated for GAPS 2005-2007 and GAPS 2011/2014 for all samples with both Endosulfan I and Endosulfan II above MDL. The plot depicts the single data points and the boxplots marking the median, 25th and 75th percentile (whiskers marking the 10th and 90th percentile).

Site types: PO= polar, BA = background, RU = rural, AG = agricultural, UR = urban

UNEP regional groups: Africa = African Group, Asia = Asia and Pacific Group, CEE = Central and Eastern European Group, GRULAC = Group of Latin America and Caribbean countries, WEOG = Western European and Others Group

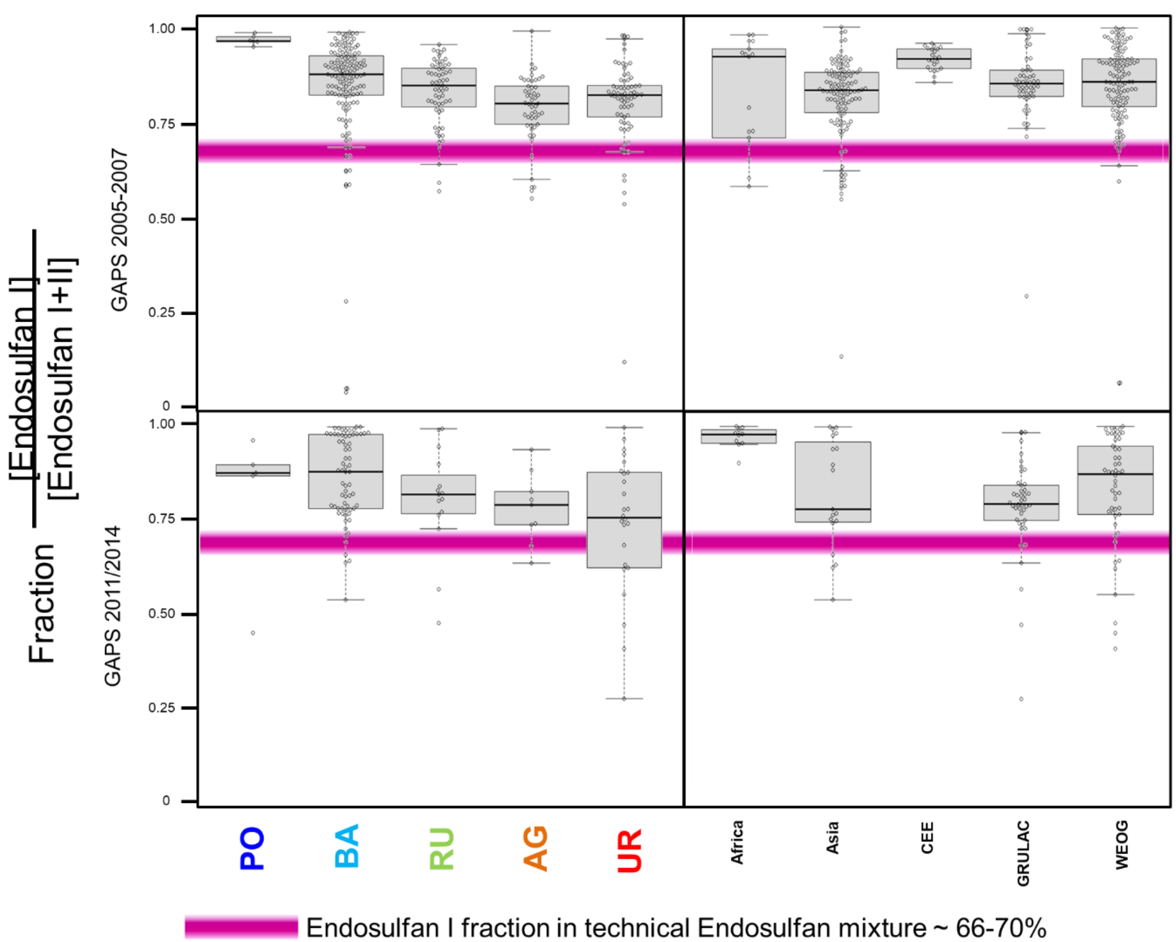

Figure S10. Bee swarm-boxplot-summary of the temporal trend slopes of the individual PCB congeners PCB 28, PCB 52, PCB 101, PCB 118, PCB 153 and PCB 180 2005-2014

The temporal trend slopes were estimated with Theil-Sen regression for the 40 GAPS sites with sufficient data. The plot depicts the single data points and the boxplots marking the median, 25th and 75th percentile (whiskers marking the 10th and 90th percentile). The windows for halving/doubling times estimated from the temporal trend slopes following first order kinetics are marked in the graph.

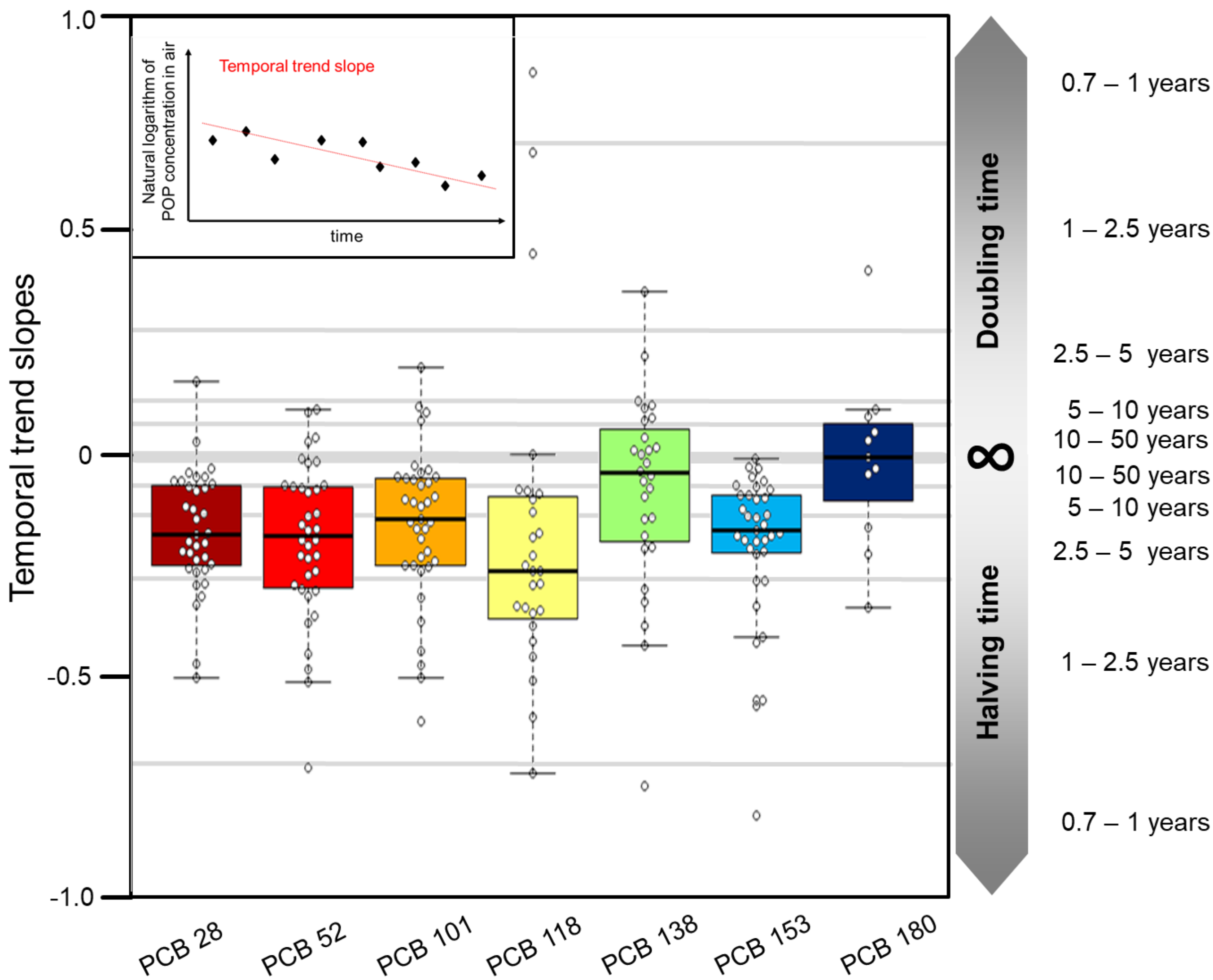

Figure S11. Bee swarm-boxplot-summary of the temporal trend slopes of Dieldrin 2005-2014

The temporal trend slopes were estimated with Theil-Sen regression for the 40 GAPS sites with sufficient data. The plot depicts the single data points and the boxplots marking the median, 25th and 75th percentile (whiskers marking the 10th and 90th percentile). The windows for halving/doubling times estimated from the temporal trend slopes following first order kinetics are marked in the graph.

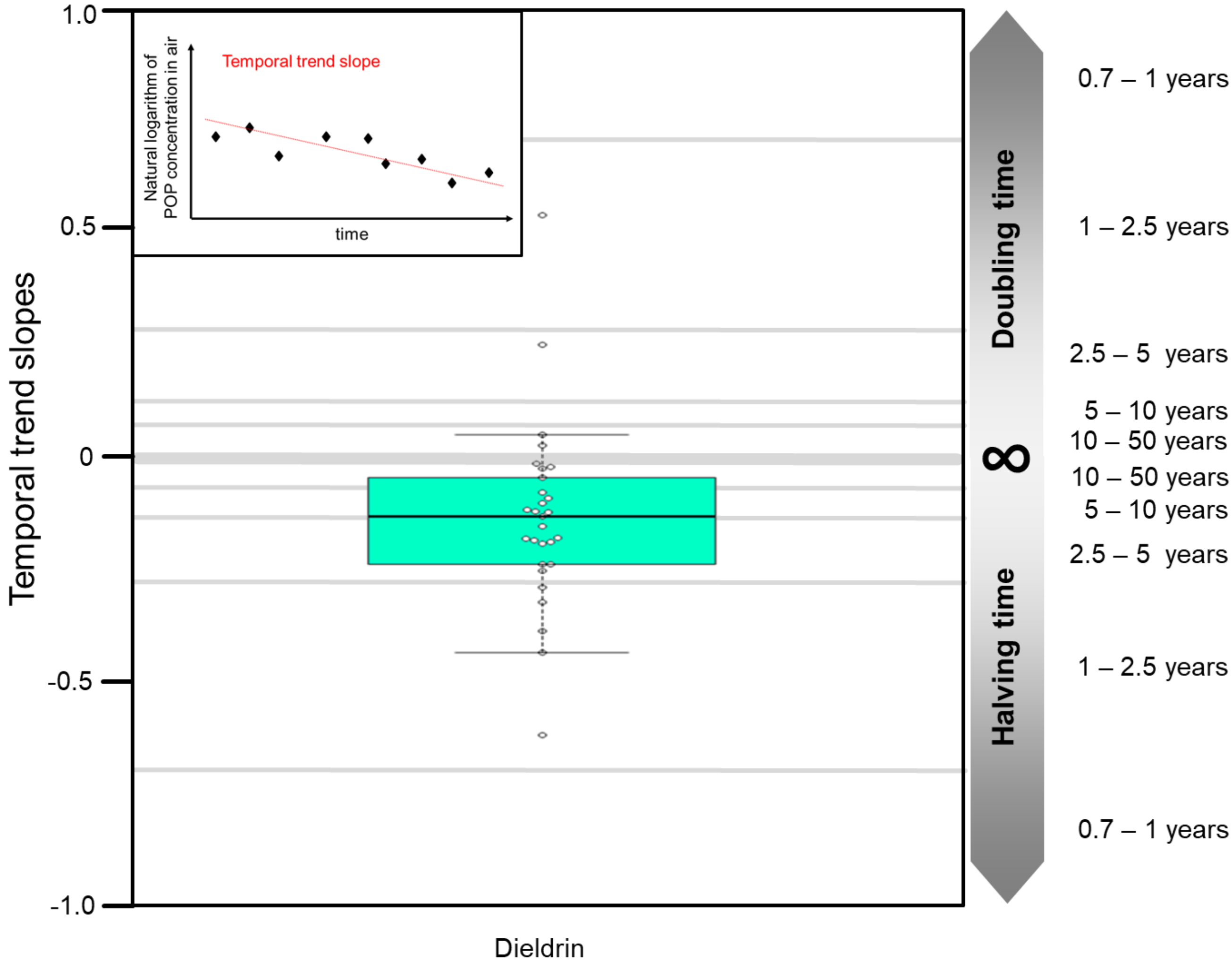

Figure S12. Bee swarm-boxplot-summary of the temporal trend slopes of *cis*-Chlordane, *trans*-Chlordane, *trans*-Nonachlor, Heptachlor and Heptachlor epoxide 2005-2014

The temporal trend slopes were estimated with Theil-Sen regression for the 40 GAPS sites with sufficient data. The plot depicts the single data points and the boxplots marking the median, 25th and 75th percentile (whiskers marking the 10th and 90th percentile). The windows for halving/doubling times estimated from the temporal trend slopes following first order kinetics are marked in the graph.

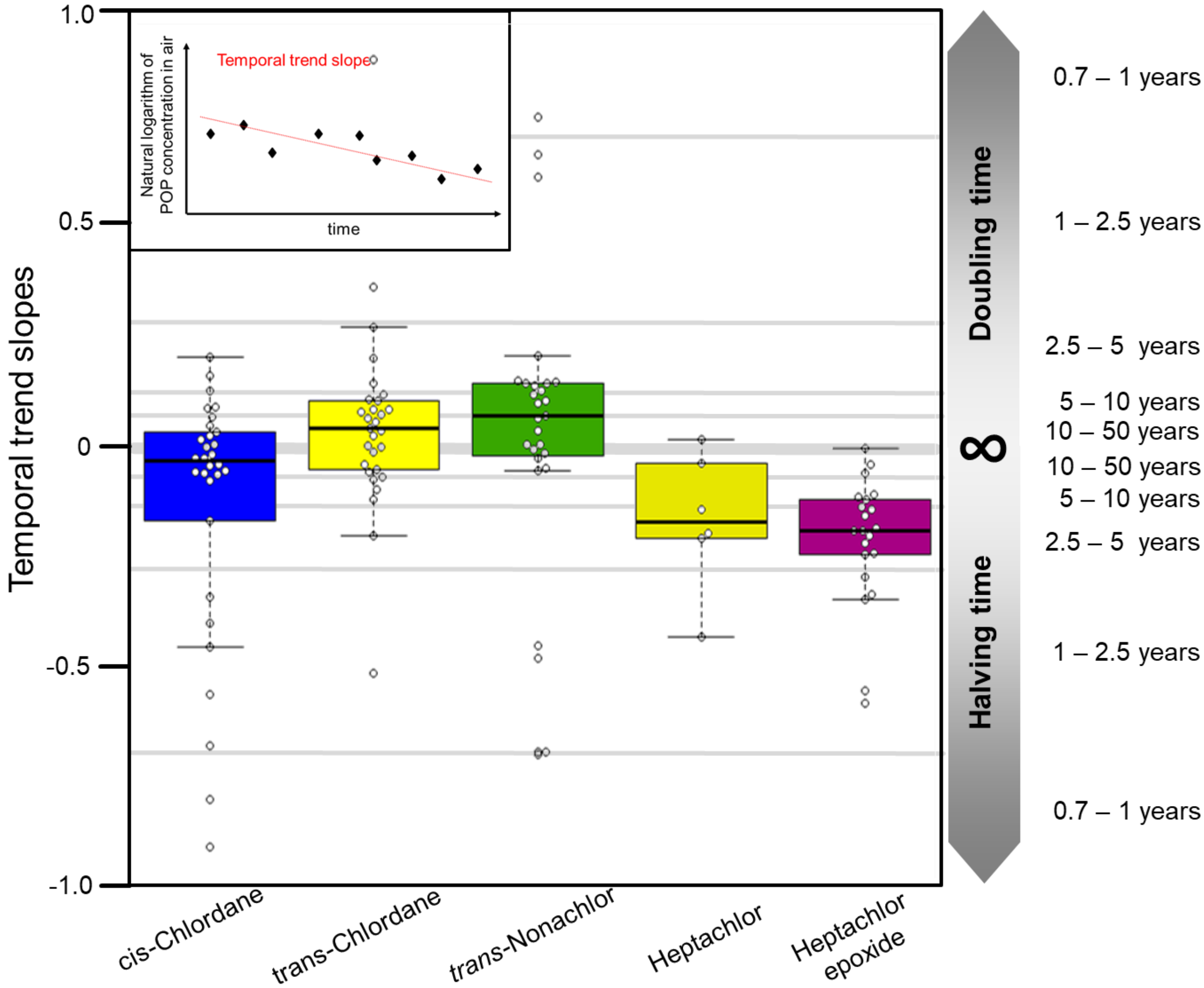

Table S1. Halving times of POPs in air reported from other studies

The majority of previous studies report declining trends and halving times for POPs in air. Where doubling times are reported, they are marked with (*).

Project	Region	Site type	Compound	Halving/doubling* time [years]
Monitoring of POPs with high volume air samplers at Alert, Pallas, Storhofdi, Zeppelin 1993-2011 Hung et al., 2016 [10]	WEOG	polar	PCBs	3.6 – 31*
			α/γ-HCH	4.1-7.7
			cis-Chlordane	12-17
			trans-Chlordane	5.9-11
			trans-Nonachlor	13-19
			Dieldrin	12-28
			Endosulfan I	37
Monitoring with high volume air samplers in the Great Lakes area 1991-2014, IADN Salamova et al., 2015 [11]	WEOG	urban	PCBs	12 - 19
			α/γ -HCH	3.9 - 4.1
			cis/trans-Chlordanes	9.0 - 12
			Endosulfan I/II	6.4 - 8.3
		background	PCBs	12.9 - 16.3
			α/γ -HCH	3.5 - 4.5
			cis/trans -Chlordanes	8.7 - 11.7
			Endosulfan I/II	7.1 - 8.9
Monitoring with medium-volume air sampler on the Tibetan Plateau 2008-2014 Wang et al., 2018 [12]	Asia and Pacific	background	α -HCH	6.1 ± 2.5
			γ -HCH	108 ± 63
			PCB 28	increasing
			PCB 52	increasing

Project	Region	Site type	Compound	Halving/doubling* time [years]
Monitoring with high volume air samplers at two EMEP sites Råö and Pallas 1996-2012 Anttila et al., 2016 [13]	WEOG	rural	PCBs	15 - 27
			α/γ -HCH	10 - 12
			cis/trans -Chlordanes	15-17
			trans -Nonachlor	19
		background	PCBs	12 - 43
			α/γ -HCH	10 - 12
			cis/trans -Chlordanes	17-21
			trans -Nonachlor	20
Monitoring with high volume air samplers in the Canadian Great Lakes Basin 1992-2012, IADN Shunthirasingham et al., 2016 [14]	WEOG	background	PCBs	9–39
			α/γ -HCH	4-5
			Endosulfan I	13
			Endosulfan II	9–11
			Endosulfan SO4	8–10
			cis/trans -Chlordanes	10-34
			trans-Nonachlor	12 - 52
			Heptachlor	5.3 - 8.6
			Heptachlor epoxide	5.8 - 12
			Dieldrin	10 - 18
Passive air sampling of POPs in West Antarctica 2011-2017 Hao et al., 2019 [15]	WEOG	polar	PCBs	2.0
			α/γ-HCH	2.0
			Endosulfan I/II	1.2
High-volume air samplers under the TOMPS network UK 1991-2012 Graf et al., 2016 [16]	WEOG	urban	PCBs	3.9 - 6.6
		rural	PCBs	5.6 - 7.5

Project	Region	Site type	Compound	Halving/doubling* time [years]
Comparison of passive (MONET) and high volume air samplers (EMEP) 2012 – 2016 Kalina et al. 2019 [17]	Europe	background	PCBs	2 – 118*
			α/γ-HCH	2 – 20
Passive air sampling in African countries (MONET) 2008-2019 White et al. 2020 [18]	Africa	background-urban	PCBs	3 – 18
			α/γ-HCH	2.3 – 23
			cis/trans -Chlordanes	2.6 – 100*
			Heptachlor	2.1 – 6.5*
			Dieldrin	0.9 – 22*
			Endosulfan I/II	0.9 – 17*
			Endosulfan SO_4	1.0 – 3.7

Figure S13. Global concentrations and decline trends of $\sum_7$PCB 2005-2014

The plot represents the geometric mean concentration for the 20 GAPS sites with long term monitoring. Declining (black) and increasing (red) concentrations over time are marked as arrows (scaled to the temporal trend slopes).

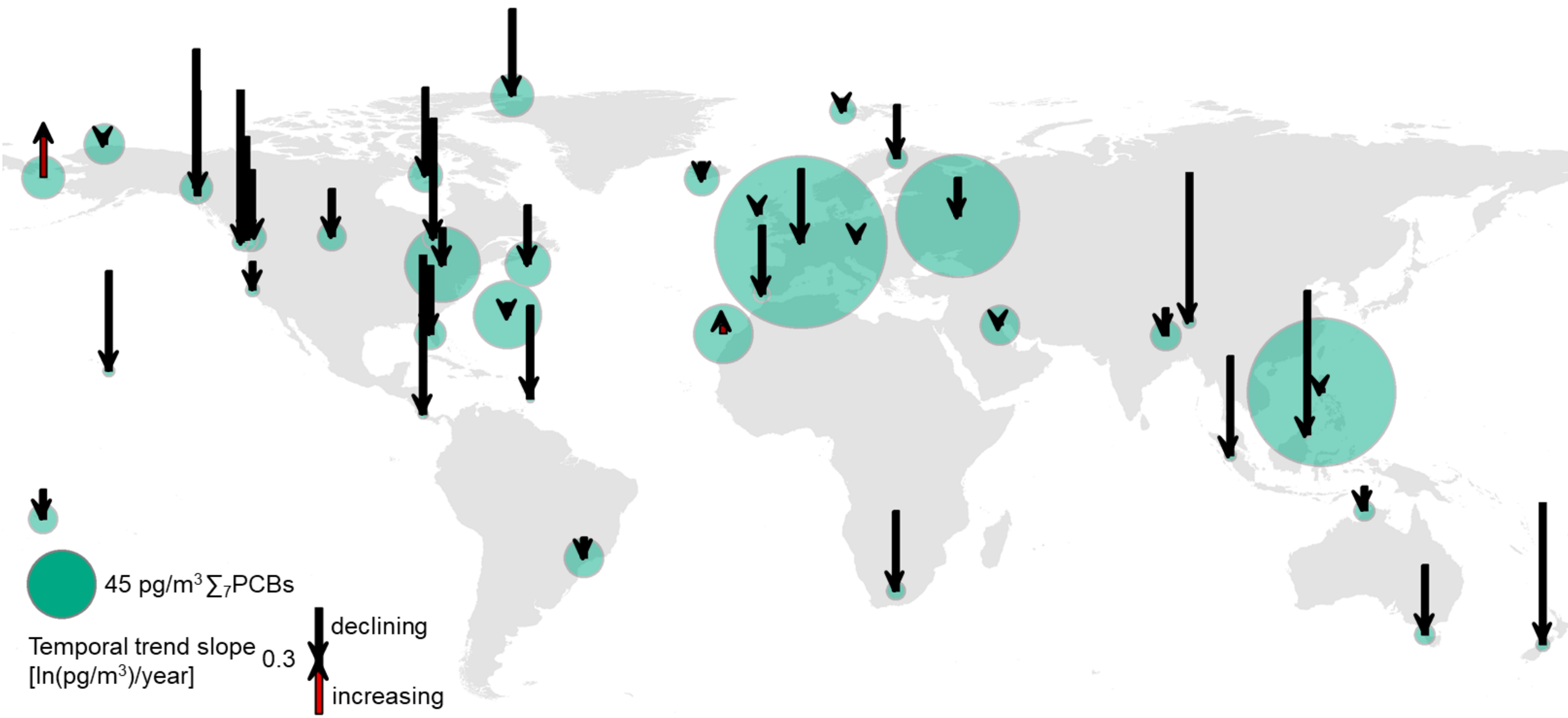

Figure S14. Global concentrations and decline trends of α-HCH 2005-2014

The plot represents the geometric mean concentration for the 20 GAPS sites with long term monitoring. Declining (black) and increasing (red) concentrations over time are marked as arrows (scaled to the temporal trend slopes).

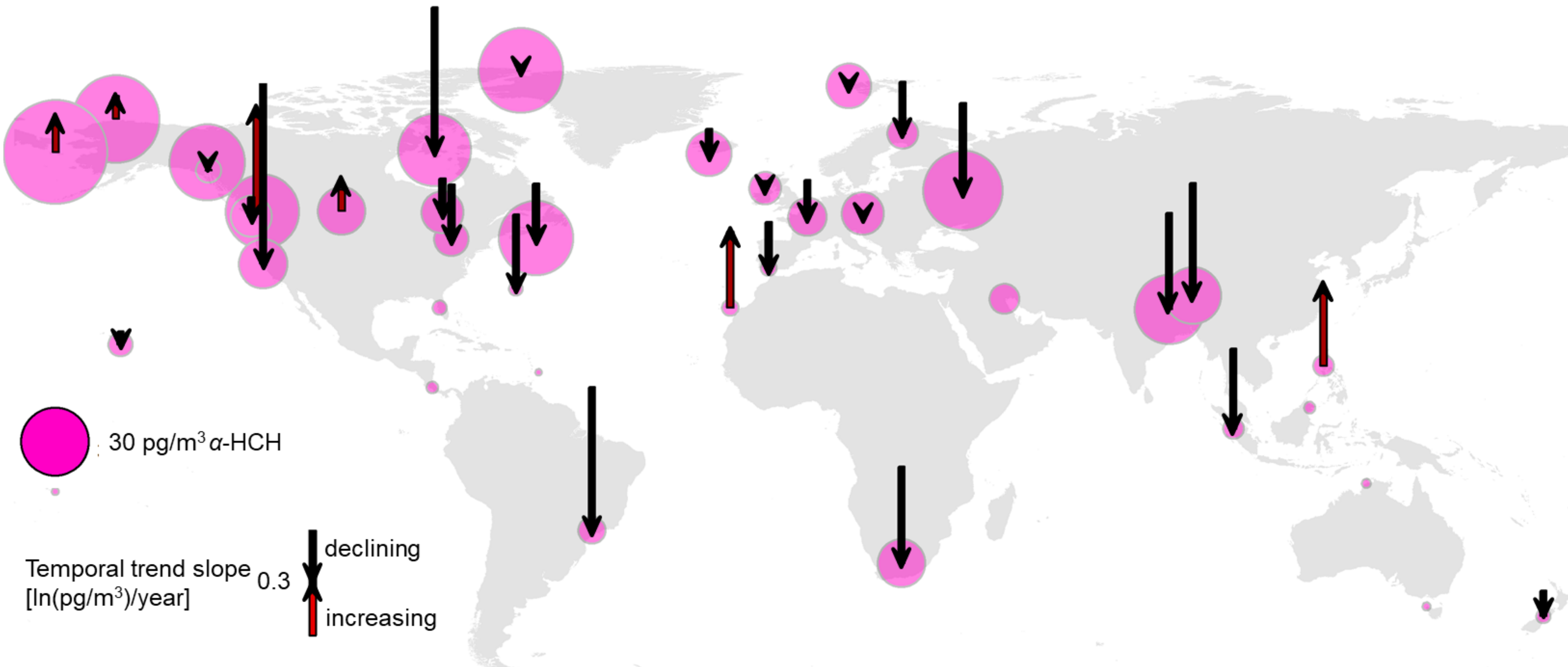

Figure S15. Global concentrations and decline trends of γ-HCH 2005-2014

The plot represents the geometric mean concentration for the 20 GAPS sites with long term monitoring. Declining (black) and increasing (red) concentrations over time are marked as arrows (scaled to the temporal trend slopes).

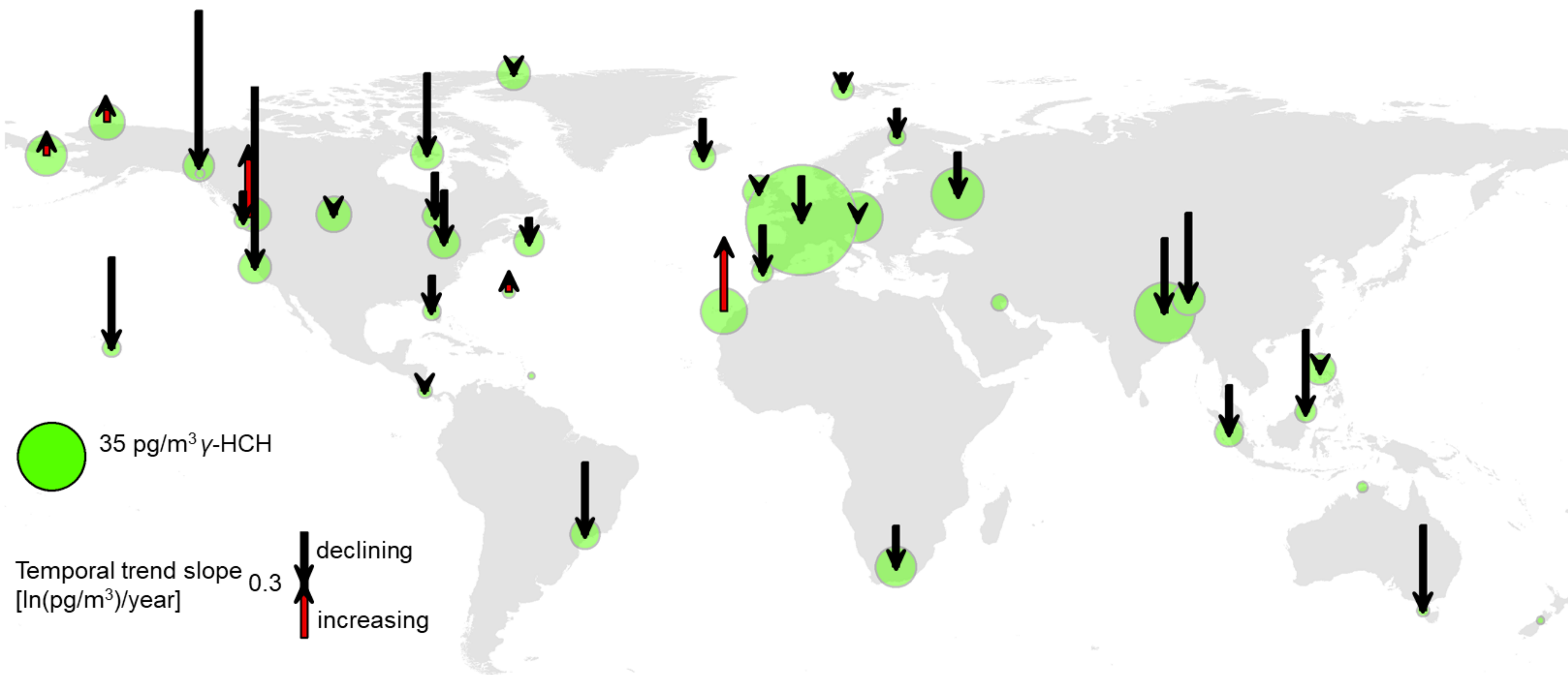

Figure S16. Global concentrations and decline trends of Endosulfan I 2005-2014

The plot represents the geometric mean concentration for the 20 GAPS sites with long term monitoring. Declining (black) and increasing (red) concentrations over time are marked as arrows (scaled to the temporal trend slopes).

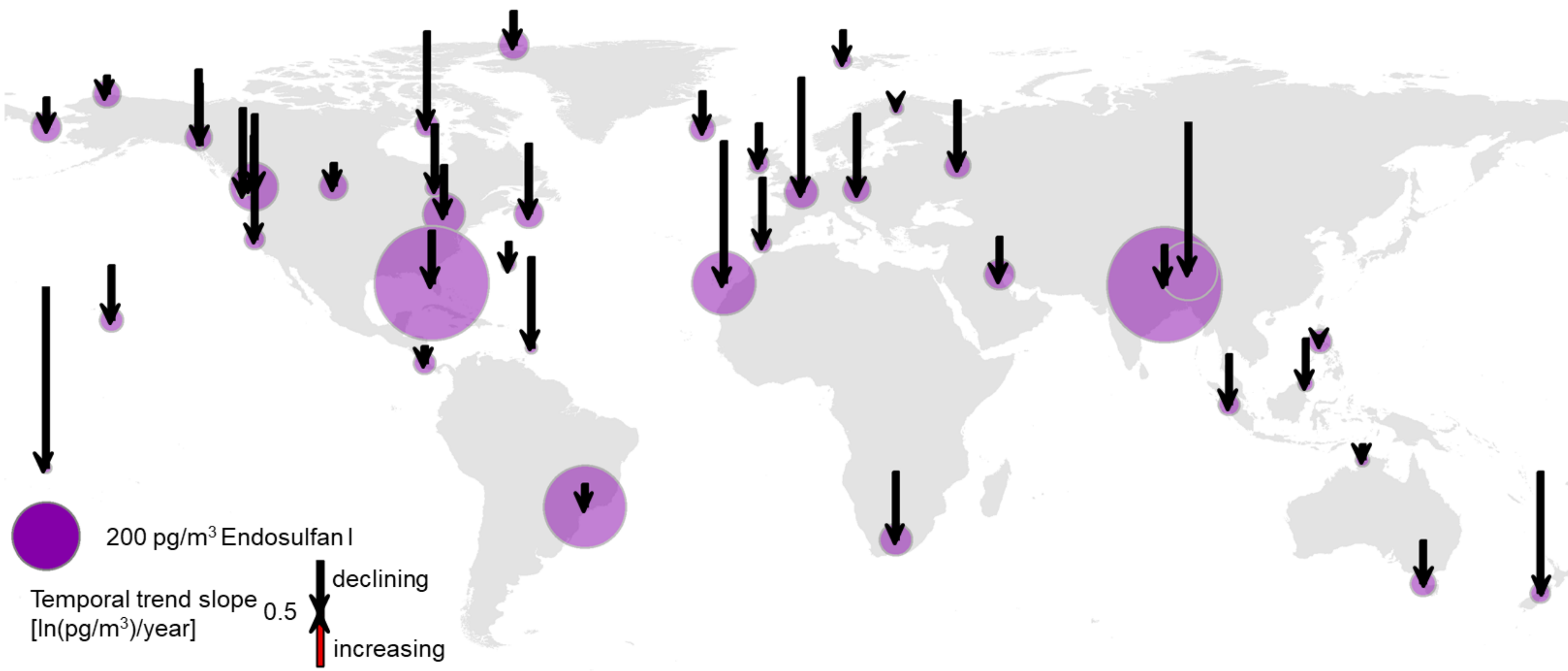

Figure S17. Global concentrations and decline trends of Endosulfan II 2005-2014

The plot represents the geometric mean concentration for the 20 GAPS sites with long term monitoring. Declining (black) and increasing (red) concentrations over time are marked as arrows (scaled to the temporal trend slopes).

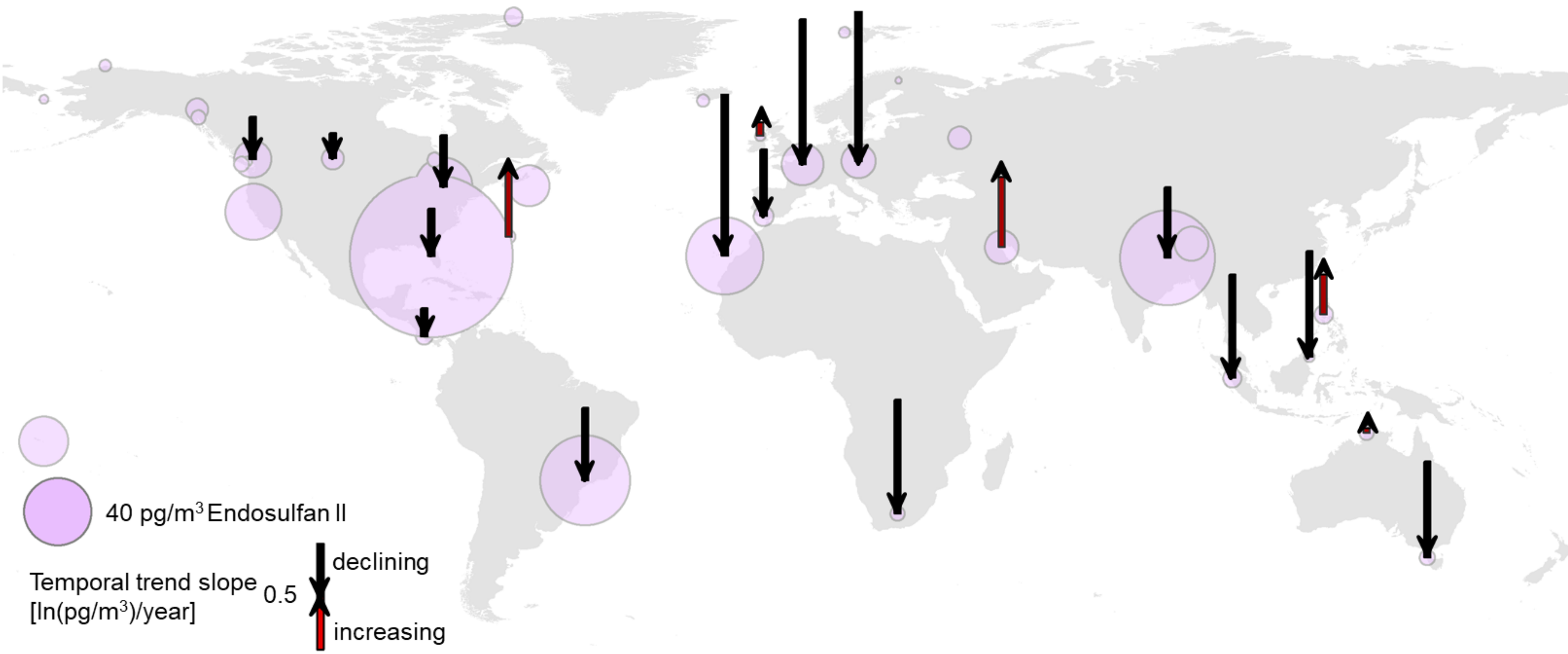

Figure S18. Global concentrations and decline trends of Endosulfan SO_4 2005-2014

The plot represents the geometric mean concentration for the 20 GAPS sites with long term monitoring. Declining (black) and increasing (red) concentrations over time are marked as arrows (scaled to the temporal trend slopes).

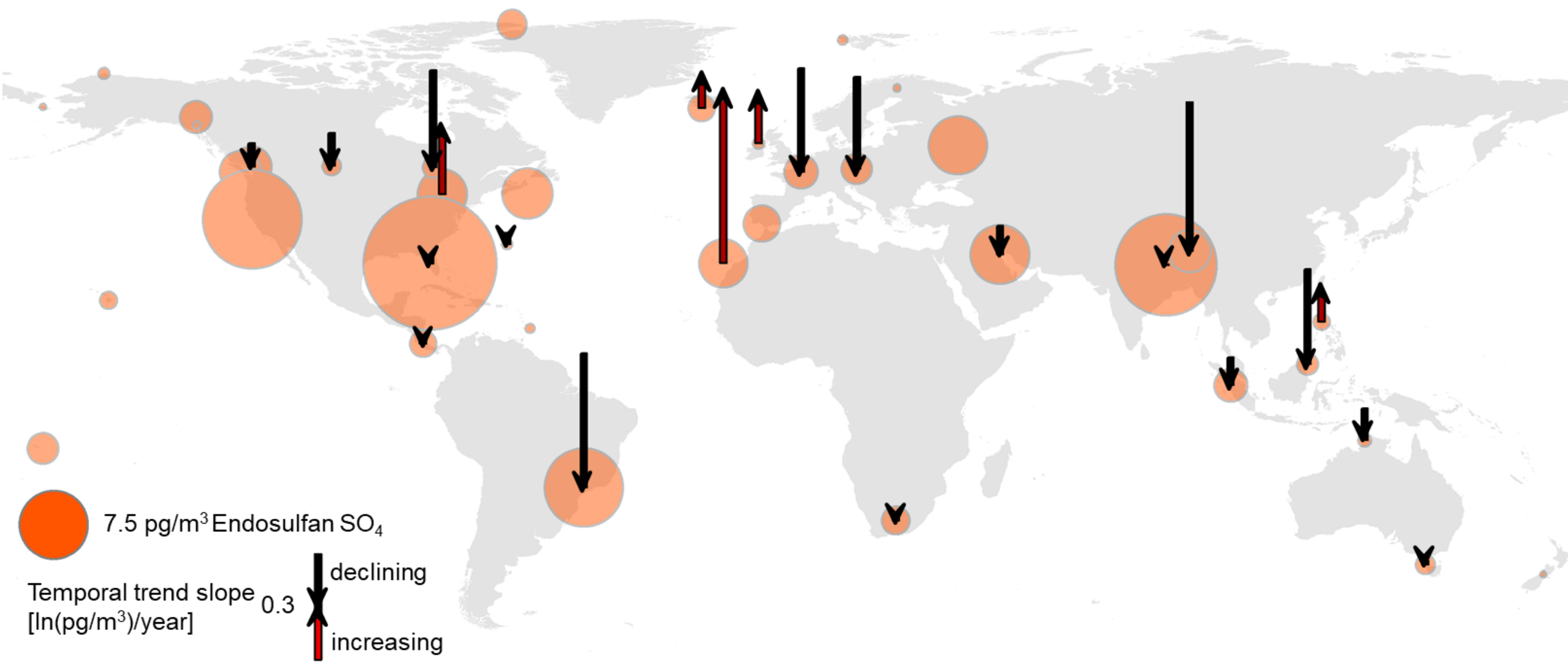

Figure S19. Global concentrations and decline trends of Dieldrin 2005-2014

The plot represents the geometric mean concentration for the 20 GAPS sites with long term monitoring. Declining (black) and increasing (red) concentrations over time are marked as arrows (scaled to the temporal trend slopes).

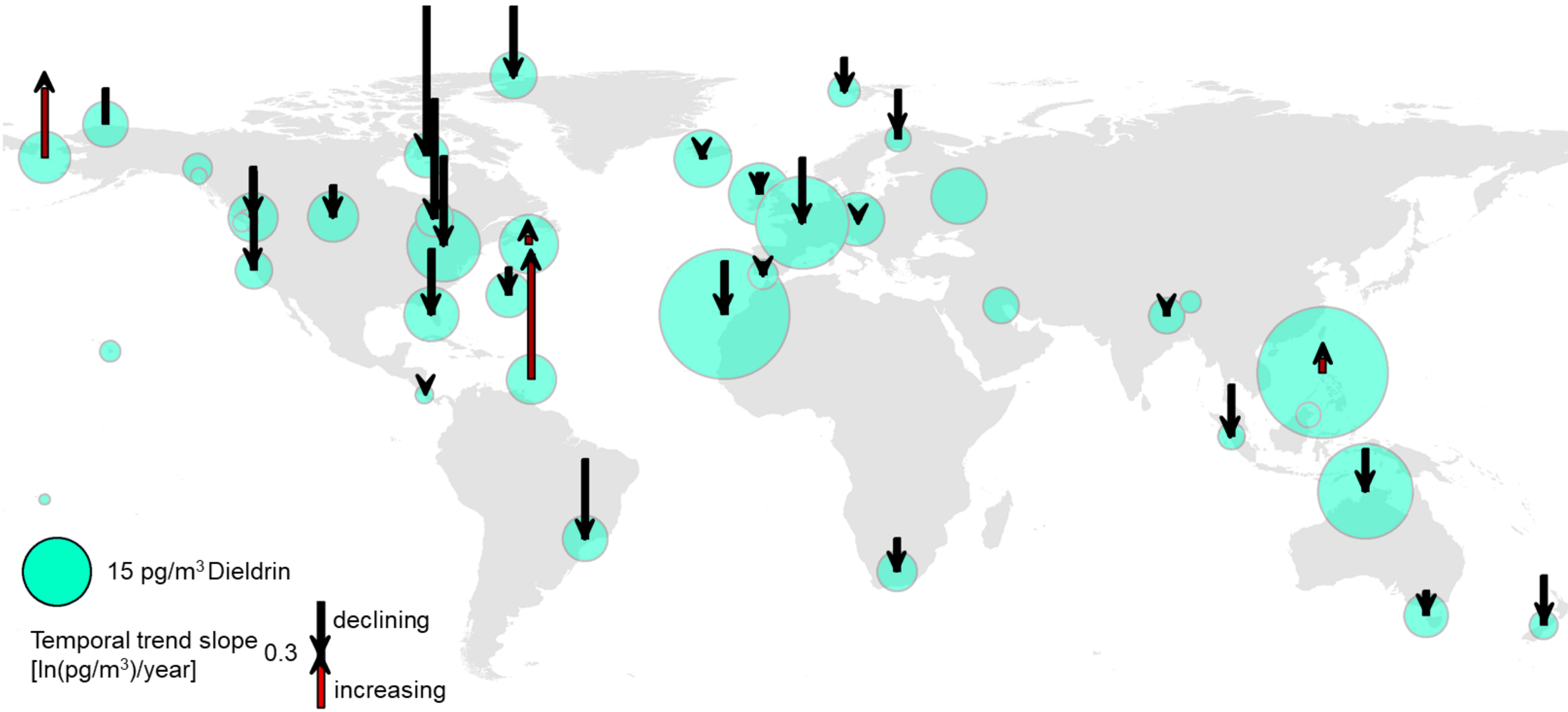

Figure S20. Global concentrations and decline trends of cis-Chlordane 2005-2014

The plot represents the geometric mean concentration for the 20 GAPS sites with long term monitoring. Declining (black) and increasing (red) concentrations over time are marked as arrows (scaled to the temporal trend slopes).

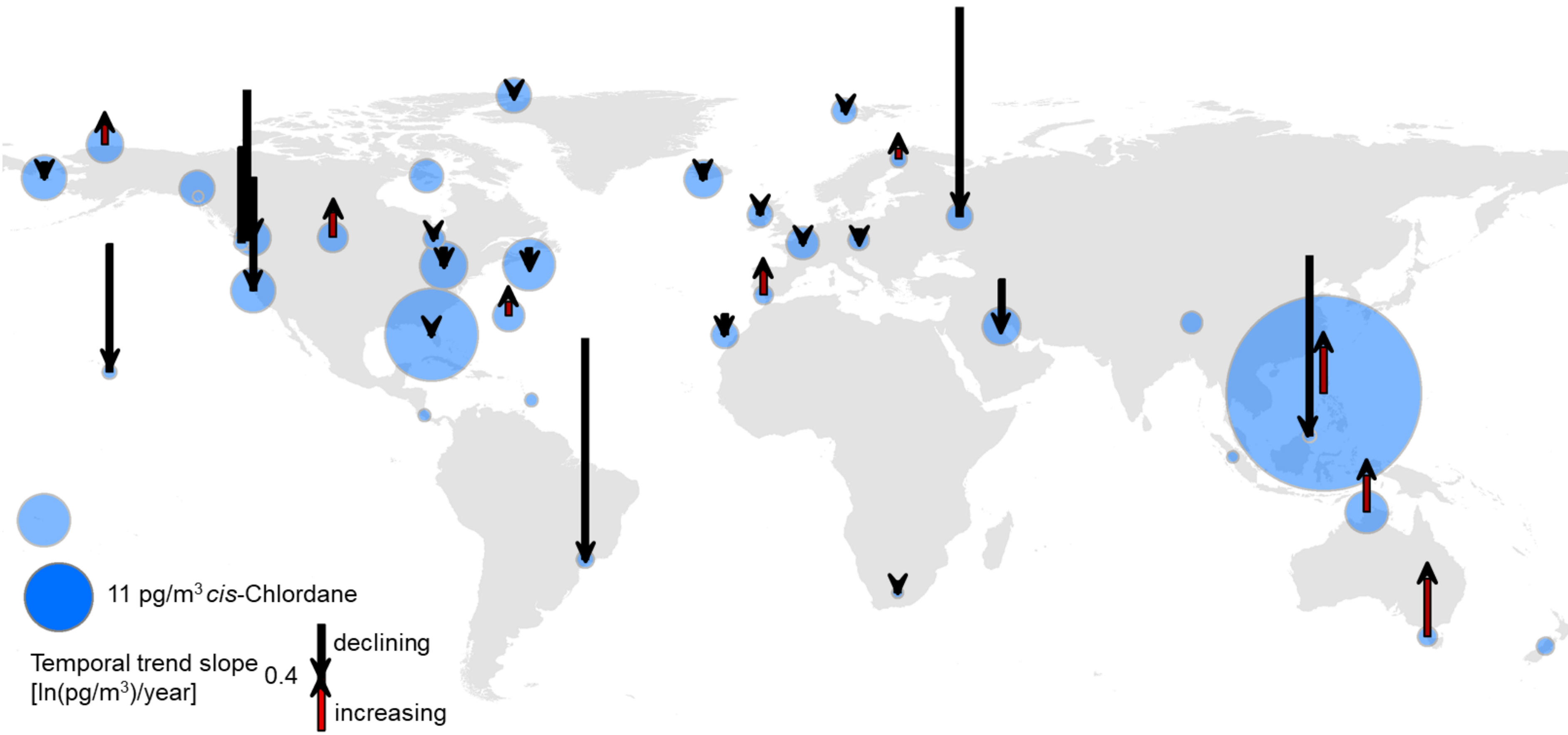

Figure S21. Global concentrations and decline trends of trans-Chlordane 2005-2014

The plot represents the geometric mean concentration for the 20 GAPS sites with long term monitoring. Declining (black) and increasing (red) concentrations over time are marked as arrows (scaled to the temporal trend slopes).

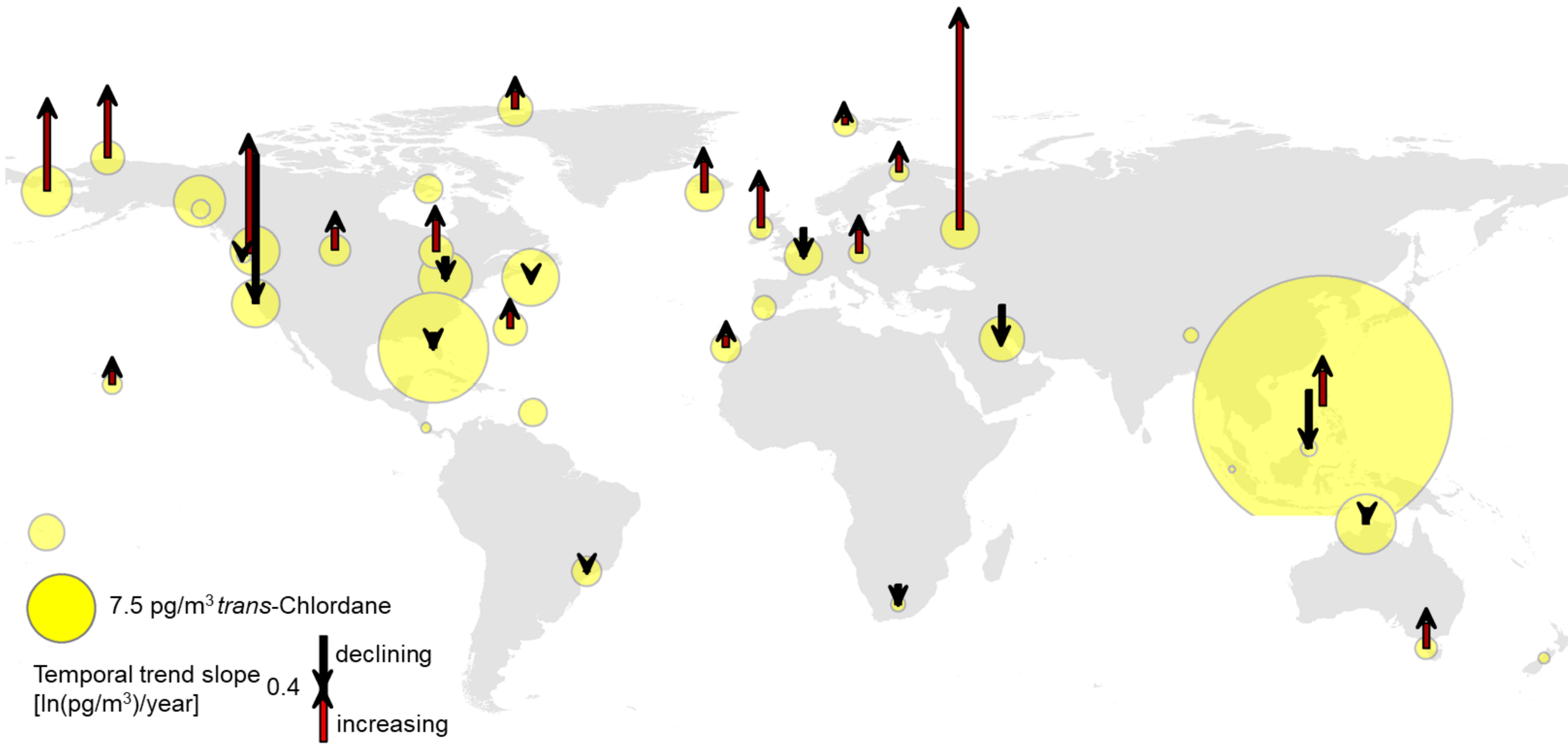

Figure S22. Global concentrations and decline trends of trans-Nonachlor 2005-2014

The plot represents the geometric mean concentration for the 20 GAPS sites with long term monitoring. Declining (black) and increasing (red) concentrations over time are marked as arrows (scaled to the temporal trend slopes).

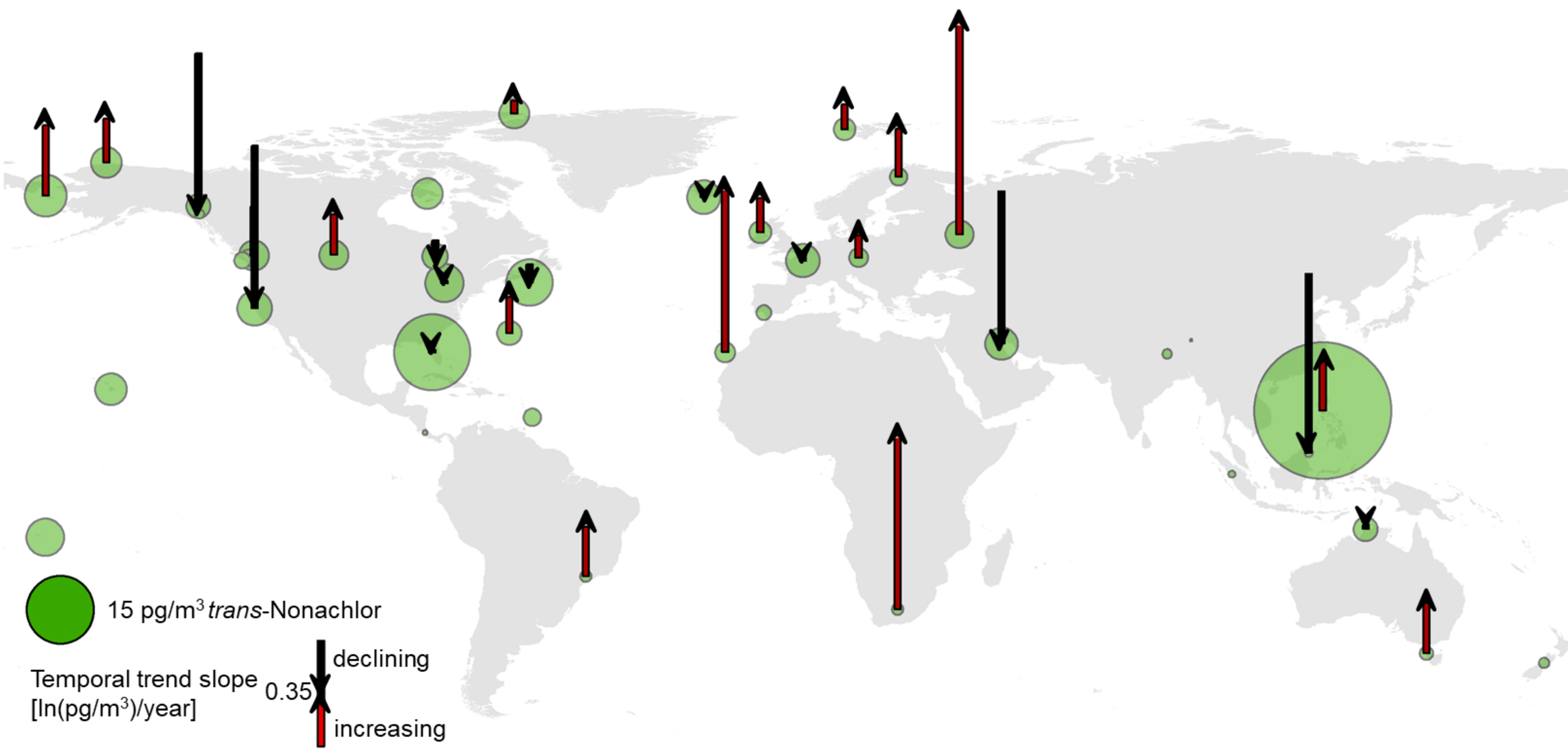

Figure S23. Global concentrations and decline trends of Heptachlor 2005-2014

The plot represents the geometric mean concentration for the 20 GAPS sites with long term monitoring. Declining (black) and increasing (red) concentrations over time are marked as arrows (scaled to the temporal trend slopes).

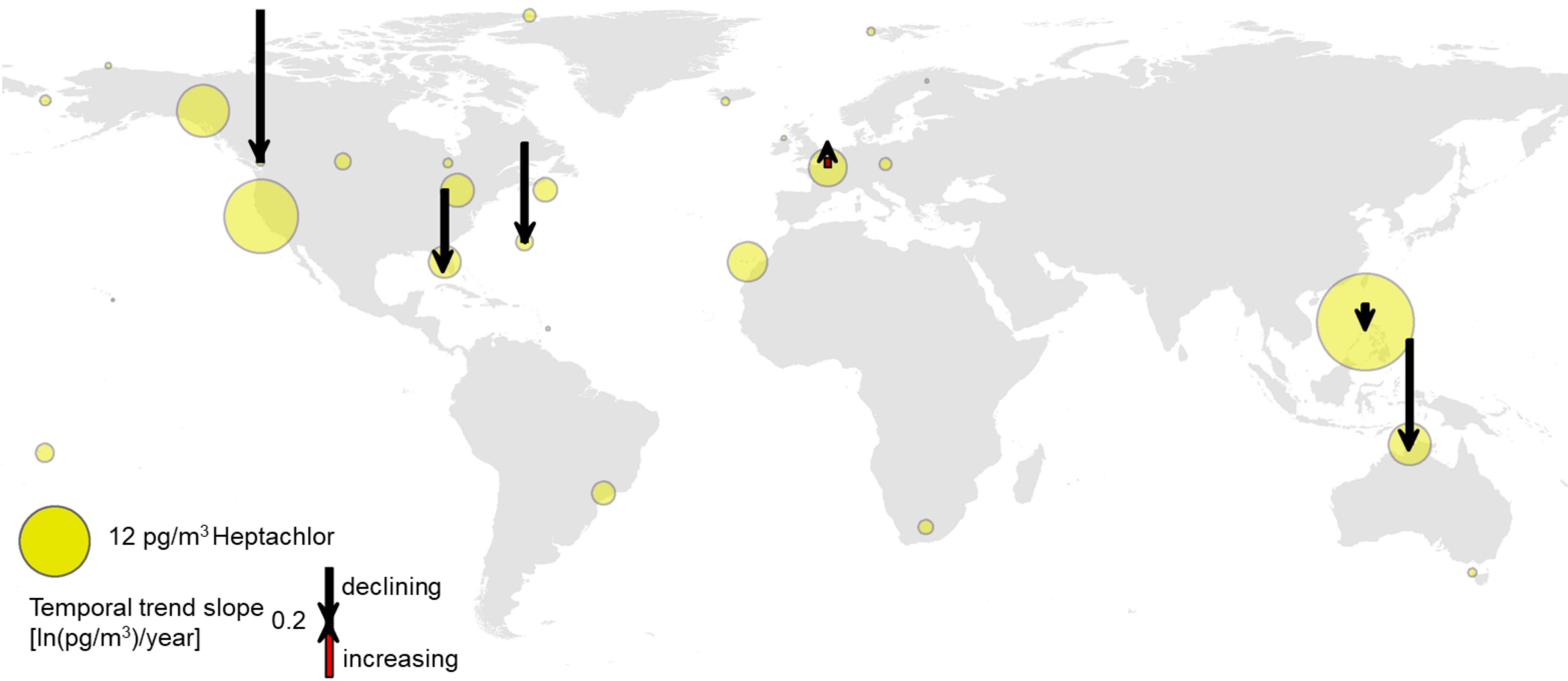

Figure S24. Global concentrations and decline trends of Heptachlor epoxide 2005-2014

The plot represents the geometric mean concentration for the 20 GAPS sites with long term monitoring. Declining (black) and increasing (red) concentrations over time are marked as arrows (scaled to the temporal trend slopes).

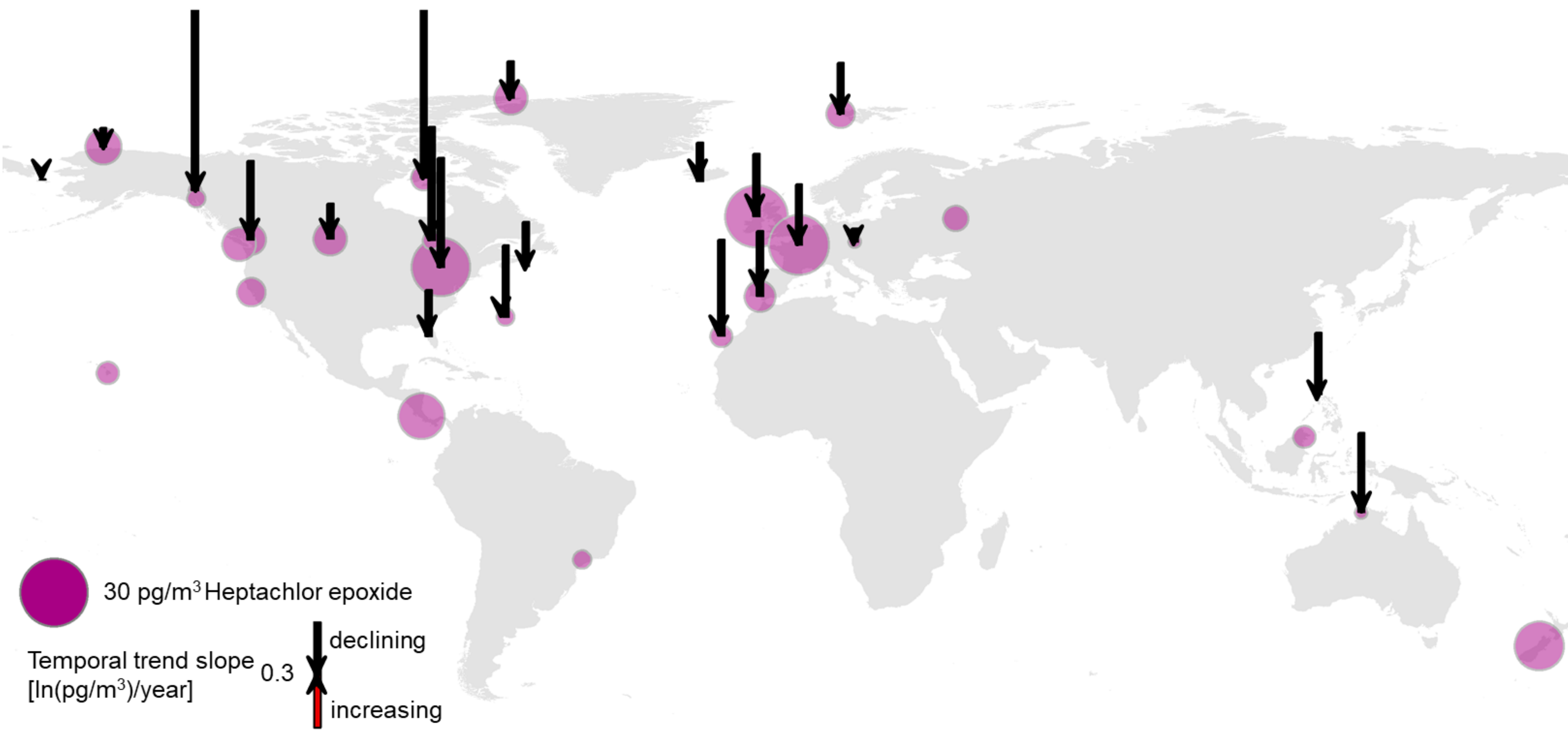

Table S2. Wilcoxon Rank Sum Test groupings of POPs based on temporal trends

p-values below 0.05 (white cells) indicate that temporal trends between compared compounds are significantly different.

	α-HCH	*cis*-Chlordane	Dieldrin	Endosulfan I	Endosulfan II	Endosulfan SO_4	γ-HCH	Heptachlor	Heptachlor epoxide	$\sum_7$PCB	*trans*-Chlordane	*trans*-Nonachlor
α-HCH	x	6.1E-01	1.6E-01	2.8E-05	5.0E-02	7.8E-01	5.0E-01	3.5E-01	5.5E-03	1.2E-02	4.8E-03	1.0E-02
cis-Chlordane	6.1E-01	x	1.3E-01	6.3E-04	1.7E-01	8.6E-01	2.0E-01	3.5E-01	1.3E-02	2.2E-02	5.0E-02	2.1E-02
Dieldrin	1.6E-01	1.3E-01	x	9.3E-03	1.9E-01	2.0E-01	4.6E-01	7.5E-01	1.9E-01	3.5E-01	1.6E-04	1.9E-03
Endosulfan I	2.8E-05	6.3E-04	9.3E-03	x	8.2E-01	8.6E-04	1.5E-04	2.5E-01	2.6E-01	1.0E-01	7.3E-10	2.8E-06
Endosulfan II	5.0E-02	1.7E-01	1.9E-01	8.2E-01	x	8.4E-02	8.6E-02	5.7E-01	6.4E-01	5.5E-01	2.1E-03	1.8E-02
Endosulfan SO_4	7.8E-01	8.6E-01	2.0E-01	8.6E-04	8.4E-02	x	4.6E-01	4.1E-01	2.0E-02	4.2E-02	4.0E-02	4.2E-02
γ-HCH	5.0E-01	2.0E-01	4.6E-01	1.5E-04	8.6E-02	4.6E-01	x	5.5E-01	2.3E-02	5.3E-02	1.9E-04	1.6E-03
Heptachlor	3.5E-01	3.5E-01	7.5E-01	2.5E-01	5.7E-01	4.1E-01	5.5E-01	x	6.4E-01	6.4E-01	1.9E-02	5.0E-02
Heptachlor epoxide	5.5E-03	1.3E-02	1.9E-01	2.6E-01	6.4E-01	2.0E-02	2.3E-02	6.4E-01	x	7.2E-01	1.6E-06	1.5E-04
$\sum_7$PCB	1.2E-02	2.2E-02	3.5E-01	1.0E-01	5.5E-01	4.2E-02	5.3E-02	6.4E-01	7.2E-01	x	1.6E-06	5.0E-05
trans-Chlordane	4.8E-03	5.0E-02	1.6E-04	7.3E-10	2.1E-03	4.0E-02	1.9E-04	1.9E-02	1.6E-06	1.6E-06	x	5.5E-01
trans-Nonachlor	1.0E-02	2.1E-02	1.9E-03	2.8E-06	1.8E-02	4.2E-02	1.6E-03	5.0E-02	1.5E-04	5.0E-05	5.5E-01	x

Figure S25. PCA of the temporal trends slopes of all congeners

Principle component analysis (PCA) was applied to the temporal trend slopes at the individual sites (n=29, sites with <50% data were excluded from the PCA)

Figure S25a. Scores plot

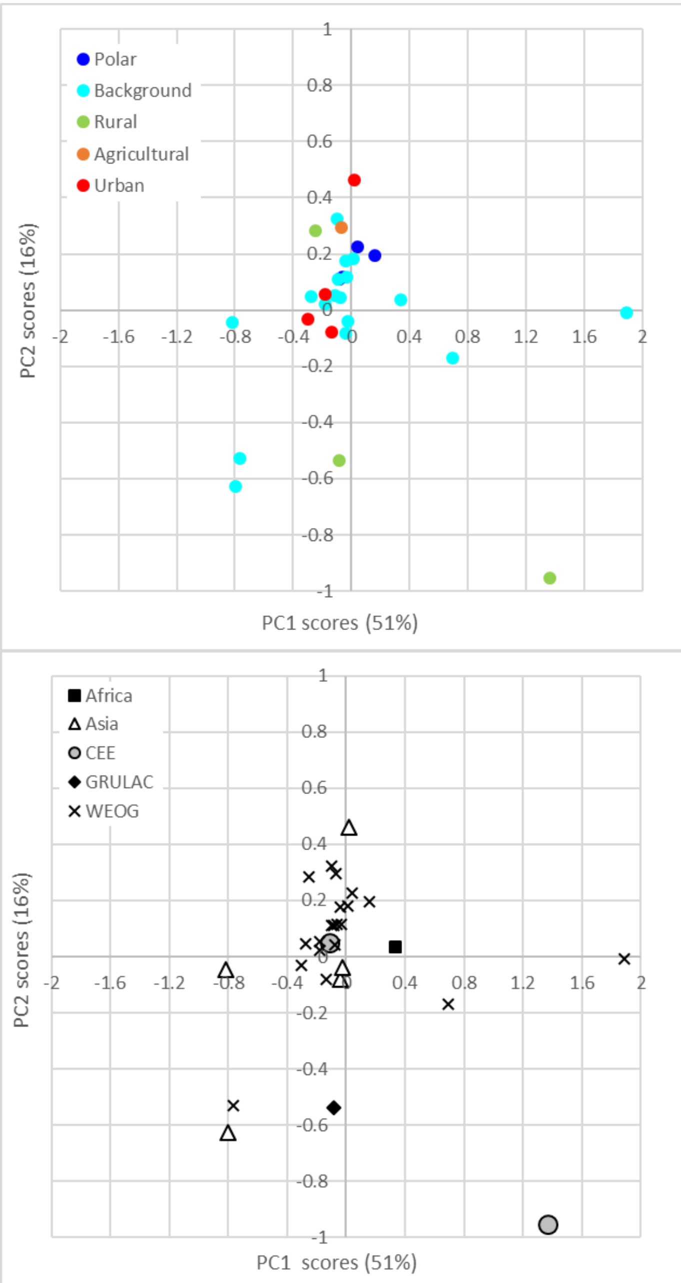

Figure S25a. Loadings plot

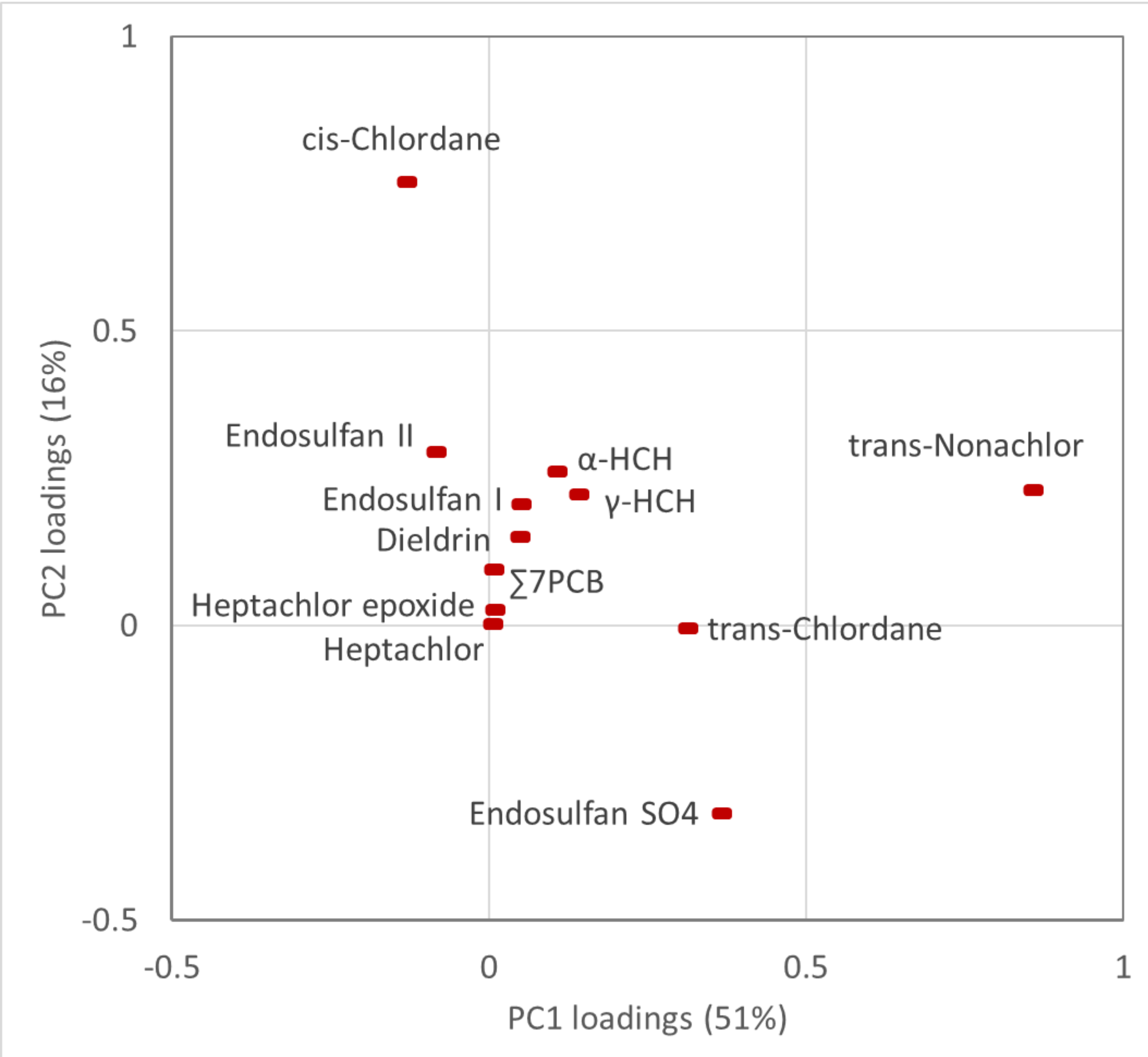

References

1. Kobayashi, T.; Tateishi, R.; Alsaaideh, B.; Sharma, R. C.; Wakaizumi, T.; Miyamoto, D.; Bai, X.; Long, B. D.; Gegentana, G.; Maitiniyazi, A.; Shirahata, T.; Mi, L.; Iizuka, K.; Yusupujiang, A.; Rinawan, F. R.; Bhattarai, R.; Dong, P., Production of Global Land Cover Data–GLCNMO2013. *Journal of Geography and Geology* **2017,** *9*, (3).
2. Pozo, K.; Harner, T.; Wania, F.; Muir, D. C.; Jones, K. C.; Barrie, L. A., Toward a global network for persistent organic pollutants in air: results from the GAPS study. *Environmental science & technology* **2006,** *40*, (16), 4867-4873.
3. Herkert, N. J.; Martinez, A.; Hornbuckle, K. C., A Model Using Local Weather Data to Determine the Effective Sampling Volume for PCB Congeners Collected on Passive Air Samplers. *Environmental Science & Technology* **2016,** *50*, (13), 6690-6697.
4. Herkert, N. J.; Spak, S. N.; Smith, A.; Schuster, J. K.; Harner, T.; Martinez, A.; Hornbuckle, K. C., Calibration and evaluation of PUF-PAS sampling rates across the Global Atmospheric Passive Sampling (GAPS) network. *Environmental Science: Processes & Impacts* **2018**.
5. The University of Iowa PUF-PAS Sampling Rate Model Interface. http://s-iihr41.iihr.uiowa.edu/pufpas_model/ (January 2020),
6. Moeckel, C.; Harner, T.; Nizzetto, L.; Strandberg, B.; Lindroth, A.; Jones, K. C., Use of depuration compounds in passive air samplers: Results from active sampling-supported field deployment, potential uses, and recommendations. *Environmental science & technology* **2009,** *43*, (9), 3227-3232.
7. National Oceanic and Atmospheric Administration (NOAA) Integrated Surface Hourly Database (ISH/ISD) Ver2. https://www.ncdc.noaa.gov/has/HAS.FileAppRouter?datasetname=3505v2&subqueryby=STATION&applname=&outdest=FILE (April 2020),
8. Harner, T. 2014_GAPS Template for calculating PUF and SIP disk sample air volumes_November 6. (January 2020),
9. Shoeib, M.; Harner, T., Characterization and comparison of three passive air samplers for persistent organic pollutants. *Environmental science & technology* **2002,** *36*, (19), 4142-4151.
10. Hung, H.; Katsoyiannis, A. A.; Brorström-Lundén, E.; Olafsdottir, K.; Aas, W.; Breivik, K.; Bohlin-Nizzetto, P.; Sigurdsson, A.; Hakola, H.; Bossi, R.; Skov, H.; Sverko, E.; Barresi, E.; Fellin, P.; Wilson, S., Temporal trends of Persistent Organic Pollutants (POPs) in arctic air: 20 years of monitoring under the Arctic Monitoring and Assessment Programme (AMAP). *Environmental Pollution* **2016,** *217*, 52-61.
11. Salamova, A.; Venier, M.; Hites, R. A., Revised Temporal Trends of Persistent Organic Pollutant Concentrations in Air around the Great Lakes. *Environmental Science & Technology Letters* **2015,** *2*, (2), 20-25.
12. Wang, C.; Wang, X.; Gong, P.; Yao, T., Long-term trends of atmospheric organochlorine pollutants and polycyclic aromatic hydrocarbons over the southeastern Tibetan Plateau. *Science of The Total Environment* **2018,** *624*, 241-249.
13. Anttila, P.; Brorström-Lundén, E.; Hansson, K.; Hakola, H.; Vestenius, M., Assessment of the spatial and temporal distribution of persistent organic pollutants (POPs) in the Nordic atmosphere. *Atmospheric Environment* **2016,** *140*, 22-33.
14. Shunthirasingham, C.; Gawor, A.; Hung, H.; Brice, K. A.; Su, K.; Alexandrou, N.; Dryfhout-Clark, H.; Backus, S.; Sverko, E.; Shin, C.; Park, R.; Noronha, R., Atmospheric concentrations and loadings of organochlorine pesticides and polychlorinated biphenyls in the Canadian Great Lakes Basin (GLB): Spatial and temporal analysis (1992–2012). *Environmental Pollution* **2016,** *217*, 124-133.
15. Hao, Y.; Li, Y.; Han, X.; Wang, T.; Yang, R.; Wang, P.; Xiao, K.; Li, W.; Lu, H.; Fu, J.; Wang, Y.; Shi, J.; Zhang, Q.; Jiang, G., Air monitoring of polychlorinated biphenyls, polybrominated diphenyl ethers and organochlorine pesticides in West Antarctica during 2011–2017: Concentrations, temporal trends and potential sources. *Environmental Pollution* **2019,** *249*, 381-389.

16. Graf, C.; Katsoyiannis, A.; Jones, K. C.; Sweetman, A. J., The TOMPs ambient air monitoring network – Continuous data on UK air quality for over 20 years. *Environmental Pollution* **2016,** *217*, 42-51.
17. Kalina, J.; White, K. B.; Scheringer, M.; Přibylová, P.; Kukučka, P.; Audy, O.; Klánová, J., Comparability of long-term temporal trends of POPs from co-located active and passive air monitoring networks in Europe. *Environmental Science: Processes & Impacts* **2019,** *21*, (7), 1132-1142.
18. White, K. B.; Kalina, J.; Scheringer, M.; Přibylová, P.; Kukučka, P.; Kohoutek, J.; Prokeš, R.; Klánová, J., Temporal Trends of Persistent Organic Pollutants across Africa after a Decade of MONET Passive Air Sampling. *Environmental Science & Technology* **2020**.